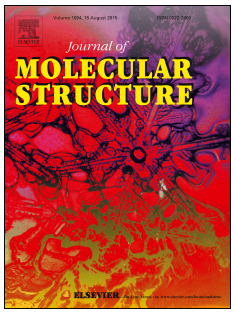

An analysis of spectroscopic, computational and biological activity studies of L-shaped sulfamoylbenzoic acid derivatives: A third order nonlinear optical material

Krishna Murthy Potla, Nuthalapati Poojith, Francisco A.P. Osório, Clodoaldo Valverde, Sampath Chinnam, P.A. Suchetan, Suneetha Vankayalapati

PII: S0022-2860(20)30395-1

DOI: https://doi.org/10.1016/j.molstruc.2020.128070

Reference: MOLSTR 128070

To appear in: *Journal of Molecular Structure*

Received Date: 13 February 2020

Revised Date: 12 March 2020

Accepted Date: 13 March 2020

Please cite this article as: K.M. Potla, N. Poojith, F.A.P. Osório, C. Valverde, S. Chinnam, P.A. Suchetan, S. Vankayalapati, An analysis of spectroscopic, computational and biological activity studies of L-shaped sulfamoylbenzoic acid derivatives: A third order nonlinear optical material, *Journal of Molecular Structure* (2020), doi: https://doi.org/10.1016/j.molstruc.2020.128070.

Credit Author Statement:

Title of the manuscript: An analysis of spectroscopic, computational and biological activity studies of L-shaped sulfamoylbenzoic acid derivatives: A third order nonlinear optical material

Krishna Murthy Potla: Design, synthesis, crystallization, perform computational calculation, interpretation of results and writing draft.

Nuthalapati Poojith: Performed bioactivity studies.

Francisco A. P. Osório: Nonlinear Optical properties calculation.

Clodoaldo Valverde: Nonlinear Optical properties calculation.

Sampath Chinnam: Spectral analysis, interpretation of results & English polishing.

P.A. Suchetan: Single crystal X-ray diffraction data analysis.

Suneetha Vankayalapati: Computational calculations, literature collection and writing draft.

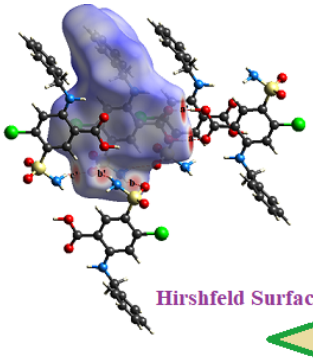

Hirshfeld Surface

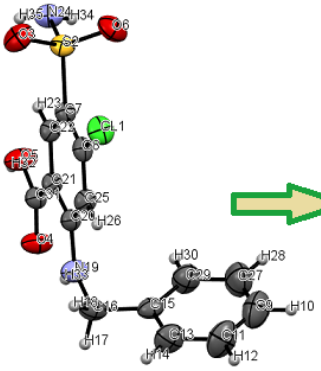

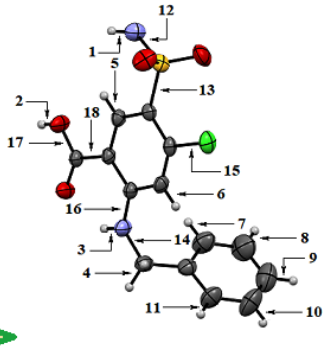

Bond Number	BDE[kcal/mol]
1.	105.07575
2.	91.57676
3.	97.12646
4.	86.73929
5.	108.86026
6.	111.54098
7.	110.62293
8.	110.5081
9.	111.02642
10.	110.5721
11.	110.20062
12.	54.08317
13.	61.777692
14.	70.643775
15.	81.530443
16.	98.135598
17.	100.41409
18.	105.12982

BDE

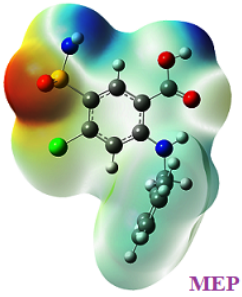

MEP

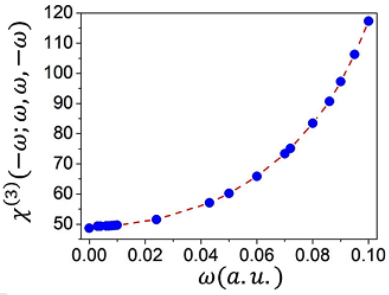

An analysis of spectroscopic, computational and biological activity studies of L-shaped sulfamoylbenzoic acid derivatives: A third order nonlinear optical material

Krishna Murthy Potla[a]*, Nuthalapati Poojith[b], Francisco A. P. Osório[c,d], Clodoaldo Valverde[e,f], Sampath Chinnam[g]**, P.A. Suchetan[h], Suneetha Vankayalapati[a,i]

[a] Department of Chemistry, Bapatla Engineering College (Autonomous), Acharya Nagarjuna University Post Graduate Research Centre, Bapatla-522 102, A.P., India.

[b] Department of Pharmacology, Sri Ramachandra Institute of Higher Education and Research, Ramachandra Nagar, Porur, Chennai, 600 116, India.

[c] Instituto de Física, Universidade Federal de Goiás, 74.690-900, Goiânia, GO, Brazil.

[d] Pontifícia Universidade Católica de Goiás, 74605-100, Goiânia, GO, Brazil.

[e]Laboratório de Modelagem Molecular Aplicada e Simulação (LaMMAS), Campus de Ciências Exatas e Tecnológicas, Universidade Estadual de Goiás, 75001-970, Anápolis, GO, Brazil.

[f] Universidade Paulista, 74845-090, Goiânia, GO, Brazil.

[g] Department of Chemistry, B.M.S. College of Engineering, Bull Temple Road, Bengaluru, Karnataka 560019, India.

[h] Department of Studies and Research in Chemistry, University College of Science, Tumkur University, Tumkur-572 103, Karnataka, India.

[i] Department of Chemistry, Bapatla College of Arts and Sciences, Baptla-522 101, A.P., India.

*Corresponding author: krishnamurthypotla@gmail.com

** Co-corresponding author: sampathchinnam@gmail.com

Abstract

The current article focuses mainly on investigation of structural, reactivity, topology studies, and third order nonlinear optical properties of the synthesized 2-(benzylamino)-4-chloro-5-sulfamoylbenzoic acid (BACSBA) with the aid of spectroscopic techniques and computational methods. The structure in the solid state was obtained unambiguously by SCXRD study that revealed that BACSBA has L-shaped structure stabilized by N-H...O intramolecular hydrogen bond. Further, the two dimensional sheet like architecture formation by linking of molecules *via* O-H...O and N-H...O hydrogen bonds, were visualized both qualitatively and quantitatively by Hirshfeld surface analysis. Also, a topological analysis made through Quantum Theory of Atoms In Molecules (QTAIM) highlights the observations N-H...O bonds on solid state. The quantum chemical calculation was performed at DFT/6-

311++G (d,p) level of basis set. The analysis of each vibrational wave number was performed with the help of potential energy distribution (PED) using VEDA4 software and correlation with experimental data shows good concurrence. The reactive sites have been predicted and visualized by molecular electrostatic surface potential (MESP) and Fukui function calculation, together with hydrogen bond dissociation energy (H-BDE) for the BACSBA compound. Frontier molecular orbitals (FMO), global reactivity parameters, natural bond orbital analysis (NBO), localized orbital locator (LOL) and electron localization function (ELF) properties have also been studied for the titled compound. The super molecule (SM) approach with 372,680 atoms at the DFT/CAM-B3LYP/6-311++G(d,p) level was used for calculating the nonlinear optical properties of the crystal. The electrical parameters such as total dipole moment, average linear polarizability and average second IDRI hyperpolarizability were calculated. In addition, the linear refractive index and the nonlinear third order macroscopic susceptibility of the crystal was estimated as a function of the frequency of the applied electric field. The value of third order nonlinear susceptibility for the BACSBA crystal at 532 nm was found to be 45.57 times greatest than the experimentally measured result of organic crystal (2E)-1-(3-bromophenyl)-3-[4(methylsulfanyl)phenyl]prop-2-en-1-one (3Br4MSP) demonstrating that BACSBA crystal could be a good potential candidate for nonlinear optical applications. In addition, the thermal stability was studied showing that the crystal as potential optical devices at temperature up to 234°C. Furthermore, preliminary studies revealed that BACSBA compound displayed promising antifungal and antioxidant activities compared with the standard drugs.

Keywords: NLO properties; reactivity analysis; SCXRD studies; biological activity; BDE calculations; sulfamoylbenzoic acid.

1. Introduction

The search for organic crystal that can be used as nonlinear optical (NLO) materials has been immensely increased in the last decade, motivated by the ease of manipulation and versatile synthetic route and by the presence of high non-linearity of these compounds [1,2]. Organic crystals have gained much importance for application in the photonic area [3,4], as well as in spectroscopy [5, 6], frequency modulators [7] and data transmission [8].

Sulfonamides (sulfa drugs) are the versatile and novel pharmacophores prevalent in nearly 200 drugs. Sulfonamide compounds have extensive applications in agricultural and pharmaceutical [9-12], nonlinear optical [13] and analytical [14], owing to their unique physicochemical and biological properties. Among a large variety of sulfonamide compounds, chlorosulfonamide moieties have great potential applications in medicinal

chemistry. Some of the chlorosulfonamide drugs used in medicine includes furosemide**(1)**, fenquizone**(2)**, metolazone**(3)**, azosemide**(4)**, chlorothiazide**(5)**, hydrochlorothiazide**(6)** (as diuretics) and diclofenamide**(7)** (as carbonic anhydrase inhibitor) (Figure 1).

Lamotte et al. reported the crystal structure of furosemide [15]. Jagadeesh et al. disclosed the ploymorphic forms of furosemide through single crystal X-ray diffraction studies [16]. Detailed investigation of X-ray structure and vibrational spectral analysis of furosemide was carried out by Bolukbasi et al. [17]. Florence, et al. performed the structure elucidation of hydrochlorothiazide by X-ray powder diffraction method [18]. Hernández et al. studied the conformational analysis of hydrochlorothiazide by theoretical studies [19]. Hydrochlorothiazide *N*,*N*-dimethylformamide solvate crystal structure was reported by Johnston et al. [20]. Fernandes et al. reported the solvate structure of chlorothiazide *N*,*N*-dimethylformamide [21]. Boopathi et al. investigated molecular structure, vibrational analysis and MEP studies of diuretic drug metolazone theoretically [22]. Porchelvi et al. reported spectroscopic and computational studies of 6-Chloro-3,4-dihydro-2*H*-1,2,4-benzothiazine-7sulphonamide1,1-dioxide (6CDBSD) [23]. Kavitha et al. reported the synthesis, spectroscopic characterization and reactivity parameter analysis of 4-chloro-3-sulfamoylbenzoic acid with antibacterial activity studies [24]. Rahman et al. performed the diuretic and anti-hypertensive studies on synthesized quinazoline derivatives [25]. Thirumalaiselvam et al. measured the Third-order nonlinear optical susceptibility of 4-methyl benzene sulfonamide single crystal by using Z-scan technique [13].

Keeping in view of the above observations, we have investigated the spectroscopic studies (SCXRD, FT-IR, FT-Raman), Hirshfeld surface analysis, QTAIM studies, computational characterizations (optimization, vibrational analysis, HOMO-LUMO analysis, MESP, Fukui calculation, ELF, LOL, BDE and H-BDE studies) of the synthesized 2-(benzylamino)-4-chloro-5-sulfamoylbenzoic acid (BACSBA). Moreover, the NLO properties of the sulfonamide BACSBA crystal was studied *via* the density functional theory (DFT) with the functional CAM-B3LYP and 6-311++G(d,p) basis set. The total dipole moment, the average linear polarizability and the average second hyperpolarizability were calculated as a function of the applied electric field frequency. From the values of these electric parameters, the dynamic linear refractive index and the dynamic third order nonlinear susceptibility was determined, and its value compared with experimental data available in the literature from Z-scan experiments. In continuation to our earlier reported works [24, 26, 27], we herein disclose nonlinear optical properties and computational as biologically potent sulfonamides and sulfonyl moieties.

2. Experimental

2.1. General

The chemicals, reagents and solvents were procured from commercial source and used directly without further purification. FT-Raman spectrum was recorded for the solid sample in the range 50-4000 cm^{-1} with resolution 2 cm^{-1} by using Nd:YAG 1064 nm laser source on BRUKER RFS 27: Stand alone FT-Raman Spectrometer (Figure S1). FT-IR spectrum was recorded for the solid sample (which is dispersed in KBr) in the range 4000-450 cm^{-1} with resolution 1 cm^{-1} on Perkin Elmer Spectrum1 FT-IR instrument with Spectrum one: FT-IR Spectrometer model (Figure S2). TG-DTA spectrum was recorded using EXSTAR TG/DTA SII 6300 instrument.

2.2. Synthesis of 2-(benzylamino)-4-chloro-5-sulfamoylbenzoic acid

1-Phenylmethanamine (0.19 mL, 1.77mmol) was taken into a 50 mL round-bottomed flask and dissolved in tetrahydrofuran (THF) as a solvent (10 mL). To this, triethylamine (0.29 mL, 2.07 mmol) was added at room temperature. Subsequently, 2,4-dichloro-5-sulfamoylbenzoic acid (0.4 g, 1.48 mmol) was added drop-wise and then refluxed for 12h. The reaction mixture was evaporated under reduced pressure and acidified with 6N HCl solution. The resulting solid was dissolved in ethyl acetate (10 mL) and washed with brine solution (3 mL). The organic layer was concentrated under reduced pressure to afford 2-(benzylamino)-4-chloro-5-sulfamoylbenzoic acid as off-white solid (0.33g, yield: 65%) (Scheme-1). Suitable crystals were grown for SCXRD studies in methanol at ambient temperature by using slow evaporation crystal growth technique.

2.3. X-ray crystallography

A colourless, needle shaped single crystal of the BACSBA compound, with dimensions of 0.25mm×0.22mm×0.18 mm was selected and mounted on a Bruker APEX-II CCD diffractometer with monochromated MoKα radiation (λ = 0.71073 Å) at 296(2) K. The data was processed with SAINT and corrected for absorption using SADABS [28]. The structure was solved by the direct method using the program SHELXT and refined by using the program SHELXS-97 [29] by full-matrix least squares technique on F^2 using anisotropic displacement parameters for all non-hydrogen atoms. The carbon bound hydrogen atoms were positioned with idealized geometry using a riding model with C–H = 0.93–0.97 Å. H atoms were refined with isotropic displacement parameters (set to 1.2 times of the U_{eq} of the parent atom). The oxygen and amino nitrogen bound H-atoms were also positioned geometrically using a riding model with O-H = 0.82 Å and N-H= 0.86 Å. The hydrogen atoms of the $–NH_2$ group were located from the difference Fourier map and were refined

freely. The *ORTEP* diagram of the compound is given in Figure 2 and the packing of molecules in the crystal lattice is shown in Figure 3. The crystallographic data and refinement parameters are summarized in Table 1. Geometric parameters for hydrogen bonds (A°) operating in the crystal structure Table 2.

2.4. Computational details

Quantum chemical calculations (optimization, vibrational frequencies, Frontier molecular orbitals (FMO), Natural bond orbital (NBO), molecular electrostatic surface potential (MESP) and bond dissociation energy (BDE) calculations) have been performed by employing density functional theory (DFT) at B3LYP/6-311++G (d,p) [30] method using the Gaussian09 software [31]. The assignments and analysis of each vibrational wave numbers were performed by using the potential energy distribution (PED) analysis using VEDA4 program [32]. A scaling factor of 0.9613 [33] had to be utilized to acquire an impressive better concurrence with the experimental data. Electron Localization Function (ELF) and Localized Orbital Function (LOL) studies were used in examining the chemical bonding between atoms of the titled compound employing Multiwfn 3.4.1 program [34].

The super molecule method (SM) was used for simulating the polarization effect of the crystalline environment around the asymmetric unit [35]. The SM is an iterative process that considers the atoms of the surrounding molecules to the asymmetric unit as point charge. The iterative process starts with the determination of the electrical charge of each atom of the asymmetric unit in vacuum, by adjusting the molecular electrostatic potential (CHELPG) at DFT/CAM-B3LYP/6-311++G (d,p) level. Then, in the position of each corresponding atom in the generated unit cells, the atoms were replaced by their partial atomic charge obtained previously. Later, the total dipole moment (μ) were determined and in the sequence the new atomic charges of the atoms of the asymmetric unit were calculated and the process was repeated until the convergence of the total dipole moment was reached [26, 36, 37] (Figure 4). Here, a bulk with 10,648 molecules totalling 372,680 atoms was built.

The SM approach has been implemented in several works for the calculation of the electric parameters as the Hyper-Rayleigh first hyperpolarizability and the third order nonlinear susceptibility and the obtained theoretical results were close to the experimental results for some organic crystal [35, 38, 39].

The dynamic average linear polarizability ($\langle\alpha(-\omega;\omega)\rangle$) and the average second hyperpolarizability associated corresponding to the dc-Kerr effect ($\langle\gamma(-\omega;\omega,0,0)\rangle$) were calculated using the expressions:

$$\langle \alpha(-\omega;\omega)\rangle = \frac{1}{3}\sum_{i=x,y,z} \alpha_{ii}\,(-\omega;\omega), \tag{1}$$

$$\langle \gamma(-\omega;\omega,0,0)\rangle = \tfrac{1}{5}\left(\gamma_{xxxx}+\gamma_{yyyy}+\gamma_{zzzz}\right)+\tfrac{1}{15}\left[\gamma_{xxyy}+\gamma_{yyxx}+\gamma_{xxzz}+\gamma_{zzxx}+\gamma_{yyzz}+\gamma_{zzyy}+4\left(\gamma_{yxyx}+\gamma_{zxzx}+\gamma_{zyzy}\right)\right]. \tag{2}$$

The linear refractive index ($n(\omega)$) was calculated using the Clausius-Mossotti equation given by,

$$\frac{n(\omega)^2-1}{n(\omega)^2+2} = \frac{4\pi}{3\,V_{uc}}\langle \alpha(-\omega;\omega)\rangle, \tag{3}$$

where V_{uc} is the unit cell volume.

The third order nonlinear susceptibility ($\chi^{(3)}(-\omega;\omega,\omega,-\omega)$) of the BACSBA crystal can be written as

$$\chi^{(3)}(-\omega;\omega,\omega,-\omega) = \left(\frac{n^2(\omega)+2}{3}\right)^4 \frac{N}{\epsilon_o\,V_{uc}}\langle \gamma(-\omega;\omega,\omega,-\omega)\rangle \tag{4}$$

In equation (4), the average second hyperpolarizability of the intensity dependent refractive index (IDRI) were calculated using the following approximation,

$$\langle \gamma(-\omega;\omega,\omega,-\omega)\rangle \cong 2\langle \gamma(-\omega;\omega,0,0)\rangle - \langle \gamma(0;0,0,0)\rangle. \tag{5}$$

All the numerical calculations were performed using the Gaussian 09 package and converted into electrostatic units (esu).

2.5. QTAIM Analysis

Topological analysis was carried out en route QTAIM methodology at the theoretical level DFT/B3LYP/6-311++G(d,p) [30] coupled in the Gaussian09 package and by Multiwfn software [34]. Based on the generated wave function, the QTAIM methodology was performed [40- 42]. In accordance with the mechanical quantum concepts the observable properties are present in the electron density [ρ(r)], which can be used with the gradient vector [∇ρ(r)] as a fundamental condition for establishing molecular topology [43, 44].

2.6. Biological activity studies

The antifungal activity of the synthesized compound BACSBA was determined against *A. Niger* (MTCC-1881), *F. oxysporum* (MTCC-1755) and *A. foetidus* (NCIM-505) by using agar disc-diffusion method [45,46]. The antioxidant activity of the synthesized compound BACSBA was determined by 1,1'-diphenyl-2-picrylhydrazyl (DPPH) [47] and Nitric oxide (NO) methods [48].

3. Results & discussion

3.1. Crystal structure analysis

The molecule was L-shaped with the dihedral angle between the two aromatic rings being 75.70(1)^{o}. The carboxylic acid group and the attached aromatic ring were in the same plane with the torsions C20-C21-C31-O4 and C20-C21-C31-O5 having values of 0.7(3) and -178.89(18)^{o} respectively. The –COOH group has syn conformation with the O-H and C=O bonds oriented in the same direction. The molecular conformation was stabilized by an intramolecular N19-H33…O4 hydrogen bond that closes into an S(6) motif.

In the crystal structure, the molecules were connected into inversion related $R^2_2(8)$ dimers *via* O5-H32…O4 hydrogen bonds. These dimers were linked to the adjacent dimers *via* a pair of N24-H35...O3 hydrogen bonds forming another $R^2_2(8)$ motif. The result of these two alternating $R^2_2(8)$ dimers was a one dimensional ribbon like architecture. The adjacent ribbons were further interconnected *via* N24-H34...O3 hydrogen bonded C4 chains that propagates along b axis to form a two dimensional sheet along ab plane.

3.2. QTAIM studies

Figure S3 shows the presence of bond critical point (BCP) for BACSBA compound interactions. The observables of each BCP is shown in **Table 3** [where [ρ(*r*)] was electron density, $[\nabla^2\rho(r)]$ was the Laplacian of electron density; V(r) is the potential energy density; H(*r*) and G(*r*) are the electronic energy density and Lagrangian kinetic energy respectively. For hydrogen bonds, $\nabla^2\rho(r)$ is positive and ρ(*r*) is small and the character of interaction can be measured by the indicators: (1) $\nabla^2\rho(r)< 0$ and H(r) < 0 ; strong interactions with covalent character, (2) $\nabla^2\rho(r)> 0$ and H(*r*) < 0 ; medium strength and (3) $\nabla^2\rho(r)> 0$ and H(*r*) > 0 ; weak interactions with electrostatic character (4) $\nabla^2\rho(r)< 0$, $\rho(r) > 0.20\ a.u.$, H(*r*) < 0 and $|V(r)| > H(r)$ interactions with covalent character [49].

The electrostatic hydrogen bonds were confirmed by the small values of ρ(r) and the positive values H(r).

Since Laplacian of electron density is positive i.e., $\nabla^2\rho(r) > 0$, the electron density is less than 0.10 a.u. (ρ(*r*) < 0.10 a.u.) and electronic energy density is positive (H(*r*) > 0).The interactions N19–H33...O4, O5–H32...O4, and N24–H34...O3 in **Table 3** were closed-shell interactions and interaction N24–H35...O3 is covalent.

3.3. Hirshfeld surface analysis

The Hirshfeld surface [50-52] and associated finger print analysis [53-55] were done with the aid of a powerful graphical tool CrystalExplorer3.1 program [56], which take crystallographic information file as an input file. The Hirshfeld surfaces and finger print plots

of the titled compound are depicted in Figure 5. The surfaces have been mapped over d_{norm}(1), *shape index* (2), *curvedness* (3) and *fragment path* (4) in the range of -0.7398 – 1.7522 Å, -1.00 – 1.00 Å, -4.00 – 0.400 and 0.00 – 14.00 Å, respectively (Figure 5). The mapped d_{norm} surfaces of the title compound shows three interactions: the first interaction between the hydrogen atom of the acid group (H3O) with the oxygen atom (O4) of the acid group, labelled as 'a' and 'a'', which was envisaged as bright red regions. The second and third interactions between hydrogen atoms (H2N1 and H1N1) of sulfonamide group with the oxygen atom (O1) of sulfonamide group labelled as 'b' and 'b'', 'c' and 'c'', which was envisaged as faint red regions. The decomposition analysis of fingerprint plots reflects that O...H/H...O (33%) interactions give the major contribution towards Hirshfeld surface and are visualized as two distinct spikes with almost equal length. The upper spike labelled as '1' corresponds to the donor spike (hydrogen atom in acid group interacting with oxygen atom of the acid group and hydrogen atoms in sulfonamide group interacting with oxygen atom of the sulfonamide group), the lower spike labelled as '2' being an acceptor spike (oxygen atom of the acid group interacting with hydrogen atom of acid group and oxygen atom of the sulfonamide group interacting with hydrogen atoms of sulfonamide groups). The second major contribution from H...H (27%) interactions appear in the middle of the scattered points in the two-dimensional fingerprint maps. The remaining contributions were mostly due to H...C (16%), H...Cl (12.1%), O...C (3.5), C...Cl (2.9%), C...C (2.4%), H...N (2.2), O...N (0.4%) and O...O (0.3%).

3.4. Optimization of geometry

The geometry optimization of BACSBA compound (Figure S4) was performed by using DFT conjugation with B3LYP/6-311++G(d,p) basis set. Optimized structure of the titled compound has ground state energy -1810.37965193 a.u. and possess C1 point group. Selected geometrical parameters, viz. bond lengths (Å), bond angles (º) and torsional angles (º) of BACSBA compound were outlined in Table 4.

The C-C bond lengths (DFT/XRD) of phenyl rings were in the range of 1.379-1.430/1.368-1.426 Å (PhI) and 1.393-1.397/1.35-1.39 Å (PhII) and for the benzene ring, the C-C bond length was 1.3993 Å [57]. The bond length of C20-N19 was 1.35620/1.346 Å (DFT/XRD), which was much shorter than the single bond C-N length 1.49 Å [58] and thereby supporting the presence of some character of a conjugation or double bond [59]. For the carboxylic group, the bond lengths were (DFT/XRD) C31-O4 = 1.22146/1.232 Å, C31-O5 = 1.35789/1.307 Å, O5-H32 = 0.96831/0.81 Å. The literature data for the similar derivatives were 1.20772/1.252 Å, 1.35213/1.273 Å, 0.96872/0.8185 Å [24], 1.201/1.208 Å, 1.359/1.304

Å, 0.96749/0.886 Å [60], which shows close agreement with that of the titled compound. The C8-C11 bond length (DFT/XRD) was 1.74327/1.7295 Å, which are in accordance with reported values 1.75083/1.720Å [24]. The bond lengths of sulfonamide group were S2-O3 = 1.45602/1.4448Å, S2-O6 = 1.45595/1.4211Å, S2-N34 = 1.66250/1.5978 Å, C7-S2 = 1.81239/1.7565 Å, which were close to the reported values 1.45235/1.4374 Å, 1.45598/1.4258 Å, 1.66847/1.5884 Å, 1.82275/ 1.78 Å [24], 1.457/1.435 Å, 1.456/1.423 Å, 1.706/1.636 Å, 1.794/1.756 Å(DFT/XRD) [27].

The bond angles around C8 atom were (DFT/XRD) C7-C8-C25 = 121.12101/121.51º, C7-C8-Cl1 = 121.33440/120.77º, C25-C8-C11 = 117.54416/117.72º and the asymmetry in angles was due to the presence of electronegative atom C11. At C31 position, the bond angles (DFT/XRD) were O4-C31-O5 = 120.33229/122.01º, C21-C31-O4 = 125.72039/123.25º, C21-C31-O5 = 113.94732/114.74º and the asymmetry in these angles confirms the existence of interactions between acid groups. The bond angles around C7, S2 and N24 positions (DFT/XRD) were C7-S2-N24, O3-S2-N24, C7-S2-O3, S2-N24-H34, S2-N24-H35 106.62024/107.80º, 105.76817/105.91º, 107.69232/107.0º, 116.96940/115.0º, 117.02003/115.0º, respectively, which show interaction between O3 atom of SO_2 group, H34 and H35 atoms of NH_2 group.

3.5. Vibrational analysis

The C8-C7-C22-C21-C20-C25 and C15-C13-C11-C9-C27-C29 rings were labelled as PhI and PhII, respectively. The computational (scaled) wave numbers, experimental FT-IR, FT-Raman bands and assignments are presented in the **Table S1**.

The carboxylic acid group was characterized by the OH stretch, C=O stretch and OH out-of-plane deformation, C-O stretch and OH in-plane deformation. For the titled compound, the OH stretching mode was theoretically observed at 3627 cm^{-1} with IR intensity 125.4641, Raman activity 174.4250 and a PED of 100%. Kavitha et al. reported the OH stretching mode for 4-chloro-3-sulfamoylbenzoic acid at 3623 cm^{-1} theoretically [24]. The carboxyl group C=O stretching vibrational mode displayed a band at 1681 cm^{-1} in the IR spectrum, 1682 cm^{-1} in the Raman spectrum, and theoretically at 1684 cm^{-1} with IR intensity 457.8412, Raman activity 103.1175 and a PED of 73 %, as expected in the region 1600-1750 cm^{-1}[61]. The bands were observed at 627 cm^{-1} (IR spectrum), 674, 643, 629 cm^{-1} (Raman spectrum) and at 672, 645, 630 cm^{-1}(theoretically) were assigned to C=O deformation modes, which was expected in the region 625±70 cm^{-1}[62]. Kavitha et al. reported the C=O deformation modes at 675cm^{-1} (Raman spectrum) and at 674, 646 cm^{-1} theoretically [24]. The O-H in-plane deformation, coupled to the C-O stretching mode is expected in the region 1390±55 cm^{-1}[61].

For the titled compound, this mode observed at 1346 cm^{-1}(theoretically), and experimentally observed at 1343 cm^{-1}(IR spectrum) and at 1342 cm^{-1}(Raman spectrum).

The frequency of vibration modes associated with NH_2 group is expected in the regions 3300-3540 cm^{-1} (stretching), 1640-1580 cm^{-1}, 1300-1100 cm^{-1} and 710-585 cm^{-1} (deformation modes), respectively [61-64]. The NH_2 group stretching frequencies were observed at 3368 cm^{-1} in the IR spectrum, 3367 cm^{-1} in the Raman spectrum and assigned theoretically at 3552 cm^{-1} with 52.3853 IR intensity, 46.3442 Raman activity and a PED of 50% (asymmetric stretching mode), and at 3283 cm^{-1} in the IR spectrum, 3279 cm^{-1} in the Raman spectrum, 3421 cm^{-1} theoretically with 49.4078 IR intensity, 97.9981 Raman activity and a PED of 50% (symmetric stretching mode). For a similar derivative, NH_2 group asymmetric stretching bands were observed at 3401 cm^{-1} (IR spectrum), 3403 cm^{-1} (Raman spectrum), 3495cm^{-1} (theoretically), and the symmetric stretching mode at 3281 cm^{-1} (IR spectrum), 3279 cm^{-1}(Raman spectrum) and 3383 cm^{-1}(theoretically) [24]. The observed difference between the calculated and experimental N-H vibrational values are 184 cm^{-1} and 185 cm^{-1} in the IR spectrum, 185 cm^{-1} and 142 cm^{-1} in the Raman spectrum, due to N-H---O interactions in solid phase. For the BACSBA compound, NH_2 group deformation modes were assigned at 1497, 990 cm^{-1} in the IR spectrum, 1497, 991 cm^{-1} in the Raman spectrum and at 1510, 992 cm^{-1} theoretically.

The vibrational modes associated with N-H group was expected in the region 3500-3300 cm^{-1} (stretching modes) and around 1500 cm^{-1} (deformation modes) [61-66]. In case of the synthesized compound (BACSBA), the N-H stretching was assigned theoretically at 3389 cm^{-1} with 172.5639 IR intensity, Raman activity 108.0501 and a PED of 99%. Kuruvilla et al. reported N-H stretching mode theoretically at 3393 cm^{-1} [67]. The deformation modes were assigned at 1416 cm^{-1} in the IR spectrum, 1558, 1417 cm^{-1} in the Raman spectrum and at 1556, 1417 cm^{-1} theoretically, which was in agreement with reported values [65].

The asymmetric and symmetric stretching vibrational mode of SO_2 group was expected in the region 1330-1295 cm^{-1} and 1150-1025 cm^{-1}, respectively [64]. For the titled compound, the asymmetric modes were observed at 1291 cm^{-1} in the IR spectrum, 1290 cm^{-1}in the Raman spectrum and theoretically at 1292 cm^{-1}, while the symmetric modes at 1083 cm^{-1} in the IR spectrum, 1080 cm^{-1} in the Raman spectrum and theoretically at 1081 cm^{-1}. These were in agreement with reported values of 1284 cm^{-1} (IR spectrum), 1285 cm^{-1} (Raman spectrum), 1286 cm^{-1} (DFT) (asymmetric) and 1090, 1072 cm^{-1} (Raman), 1090, 1071 cm^{-1} (DFT) (symmetric) [24]. The deformation modes of SO_2 group were expected in the regions - scissoring 560±40 cm^{-1}, wagging 500±55 cm^{-1} and twisting 440±50 cm^{-1} [61]. In the titled

compound, these modes were observed at 460 and 381cm^{-1} in the Raman spectrum and theoretically at 461 and 384 cm^{-1}.

The stretching vibrational modes of SN group were observed at 789 cm^{-1} in the IR spectrum, 790 cm^{-1} in the Raman spectrum and theoretically at 794 cm^{-1} with high IR intensity 114.4742, low Raman activity 9.0882 and a PED of 79% which was in accord with literature values of 785 cm^{-1} (Raman spectrum) and 782 cm^{-1} (DFT) [24].

The vibrational mode observed at 643 cm^{-1} in the Raman spectrum and calculated at 645 cm^{-1} with 44.3873 IR intensity, 12.2815 Raman activity and a PED of 19% was assigned for CS stretching vibrational mode of BACSBA compound. For the titled compound, CCl stretching modes were observed at 497 cm^{-1} (IR spectrum), 499 cm^{-1} (Raman spectrum) and theoretically at 504 cm^{-1} with a PED 20% (DFT), as expected in the region 710-505 cm^{-1}[61].

For the CH_2 groups, the stretching and deformation (scissoring, wagging, twisting and rocking) modes appear in the range 3050-2935 cm^{-1} and 1500-800 cm^{-1}, respectively [61, 62]. The CH_2 modes of the titled compound were assigned at 2943, 2901 cm^{-1} (IR), 2942, 2903 cm^{-1} (Raman), 2943, 2902 cm^{-1} (DFT) (stretching) and 1432, 1330 cm^{-1} (IR), 1431, 1329 cm^{-1} (Raman), 1436-1334 cm^{-1} (DFT) (deformation modes), which were in agreement with reported values [65].

The CH stretching modes of the aromatic rings were normally expected above 3000 cm^{-1}[61,62]. Here, these modes were displayed at 3105 cm^{-1} in the IR spectrum, 3102 cm^{-1} in the Raman spectrum and at 3106, 3104 cm^{-1} theoretically for PhI, 3065, 3040, 3030 cm^{-1} in the IR spectrum, 3060, 3039 cm^{-1} in the Raman spectrum and at 3068-3029 cm^{-1} theoretically for PhII. For aromatic rings, the CH in-plane and out-of-plane deformations were expected above and below 1000 cm^{-1}[61]. In the present case, the modes were assigned as follows: i) for PhI a) in-plane deformations at 1416, 1222 cm^{-1} (IR spectrum), 1417, 1221 cm^{-1} (Raman spectrum) and 1417, 1222 cm^{-1} (theoretically), b) out-of-plane deformations at 887, 825 cm^{-1} (IR spectrum), 885, 823 cm^{-1} (Raman spectrum), 888, 827, 826 cm^{-1} (theoretically); for PhII a) in-plane deformations at 1301, 1153, 1137 cm^{-1} (IR spectrum), 1428, 1381, 1300, 1151, 1136 cm^{-1} (Raman spectrum), theoretically in the range 1470-1137 cm^{-1}, b) out-of-plane deformations at 949, 725, 689 cm^{-1} (IR spectrum), 951, 879, 716, 688 cm^{-1} (Raman spectrum) and theoretically at 967, 952, 881, 716, 688 cm^{-1}, respectively [61].

The phenyl ring stretching modes were attributed at 1569, 1343, 1287 cm^{-1} (IR spectrum), 1571, 1342, 1285 cm^{-1} (Raman spectrum) and in the range 1572-1289 cm^{-1} (theoretically) for PhI and 1584, 1565, 1301 cm^{-1} (IR spectrum), 1584, 1563, 1300 cm^{-1} (Raman spectrum) and in the range 1584-1300 cm^{-1} (theoretically) for PhII. The ring breathing mode for PhII

(mono-substituted phenyl ring) assigned at 977 cm^{-1} in the Raman spectrum and theoretically at 978 cm^{-1} has low IR intensity (2.0156), medium Raman activity (24.2603) with a PED of 27%. These values were close to the theoretical value of 977 cm^{-1} reported by Krishna et al. [59]. The ring breathing mode was observed at 980 cm^{-1} in the Raman spectrum and at 982 cm^{-1} theoretically for PhI.

3.6. Frontier molecular orbitals analysis

Easy way for the calculation of global reactivity parameters is accounting the energy value difference between the highest occupied molecular orbital (HOMO) and the lowest unoccupied molecular orbital (LUMO) of a molecule. The combination of these orbitals commonly called as frontier molecular orbitals (FMOs) are the outmost orbitals of the molecules. The energy parameters of HOMO and LUMO are directly associated to electron donating ability and electron accepting ability of molecule, respectively, and the energy gap difference between these orbitals plays crucial role to explain reactivity parameters of the molecules. The energy values of the frontier orbitals were calculated at DFT/B3LYP/6-311G++ (d,p) method.

The depiction associated to spatial distribution of HOMO and LUMO, related energies and energy gap is summarized in Figure S5. It was observed that the HOMO (MO: 88) was confirmed over whole molecule other than amine group, chloro group and partially on methylbenzene ring; while, the LUMO (MO: 89) was localized over whole molecule other than methyl benzene ring and sulfonamide group. Consequently, computed absorption band λ_{max} = 327 nm (Figure S6) implies transition between HOMO→LUMO orbitals of the present investigated compound. The transitions, wavelength, oscillator strengths and CI coefficient calculated by DFT/B3LYP/6-311G++ (d,p) method are given in **Table S2**.

The global chemical parameters of title compound are: E_{HOMO} (88) = -6.4280 eV, E_{LUMO} (89) = -2.0779 eV, ΔE =4.3501eV, ionization potential (I) = 6.4280 eV, electron affinity (A) =2.0779 eV, electronegativity (χ) = 4.2529 eV, global hardness (η) = 2.1750 eV, chemical softness (ν) = 0.4597 eV, chemical potential (μ) = -4.2529 eV and electrophilicity index (ω) = 4.1579 eV [68]. The negative value of the chemical potential indicates that the compound was stable.

3.7. Local reactivity calculations (molecular electrostatic surface potential and Fukui function)

The molecular electrostatic surface potential (MESP) is a most commonly used quantum chemical descriptor for understanding the connection between the structure and chemical reactivity through visualisation of three-dimensional colour coding based on electron density

[69-71]. It is a unique and valuable technique for the assessment of chemical and physical parameters, particularly for pharmaceutically important molecules. Politzer et al. [72] used MESP to illustrate a variety of chemical processes like chemical reactivity, hydrogen bonding, etc. In the three-dimensional MESP plot depicted in Figure S7, electron rich regions (negative potential areas) (for instance, vicinity over un-protonated atoms like oxygen atoms of sulfonamide group, which are good hydrogen bond acceptors as well as most probable sites for electrophilic attack) were marked with red colour. On the contrary, the electron poor regions (positive potential areas) (such as vicinity over protonated atoms like hydrogen atoms of amines and acid groups, which are good hydrogen bond donors as well as most probable sites for nucleophic attack) were marked with blue colour. From these observations, it can be concluded that the SO_2 and NH_2 groups play a crucial role in the chemical and intermolecular interactions.

Parr and Yang in 1984 proposed a technique called Fukui function for examining and analysis of the most reactive sites for electrophilic or nucleophilic reactions in a molecule, when the number of electrons is altered (either addition or remove). Fukui calculations were performed by altering the multiplicity and charge. This also helps to examine the molecular polarizability, electronic structure and electrostatic potential surface [73-76].

Fukui functions can be calculated using the following equations

$f_r^- = q\,r\,(N) - q\,r\,(N-1)$ for electrophilic attack (8)

$f_r^+ = q\,r\,(N+1) - q\,r\,(N)$ for nucleophilic attack (9)

$f_r^0 = ½[q\,r\,(N+1) - q\,r\,(N-1)$ for radical attack (10)

In these equations, qr is the atomic charge at the r^{th} atomic site is the anionic (N+1), cationic (N-1) and neutral (N) molecule [77].

The local softness is related to Fukui function as follows:

$sr\text{-}fr\text{-} = Sf^-_k$ for electrophilic attack (11)

$sr\text{+}fr\text{+} = Sf^+_k$ for nucleophilic attack (12)

$sr0\ fr0 = Sf^0_k$ for radical attack (13)

From the analysis of dual descriptor, the reactive sites (nucleophilic and electrophilic) of the title compound explained. From the Table 5 values, the reactivity order for nucleophic attack C8≈C9>C31>C22>O4>C20>O5>Cl1>N24>C27>S2. On other hand, for electrophilic attack we can observe N19>C7>C25>C21>C15>O3>O6>C29>C13>C11.

3.8. Chemical Bonding Analysis (Electron Localization Function and Localized Orbital Function)

The two dimensional graphical depiction of Localized Orbital Locator (LOL) and Electron Localization Function (ELF) are shown in Figures S8 and S9. The electron localization function can be helpful to examine the electron localization in a molecular system [78]. LOL is also a similar study about the localized electron cloud. The electron localization can be calculated by applying Pauli repulsion on two like-spin electrons [79]. The bonding, reactivity and chemical structure can be studied in detail using the data [80]. For ELF, 1 (denotes with red colour) and 0 (denotes with blue colour) are the maximum and minimum limits [81].

For the examined compound, the maximum Pauli repulsion was indicated with red colour around hydrogen atoms with single electrons and carbon atoms marked by blue region shows minimum Pauli repulsion. Covalent regions marked by red colour show high LOL values, while electron depletion between valence shell and inner shell marked blue coloured areas in the Figure S8 [82].

3.9. Natural bond orbital (NBO)

Natural bond orbital (NBO) analysis was done by using NBO 3.1 program [83] actualized in the Gaussian09 suite at DFT conjugation with B3LYP/6-311++G(d,p) method, which provide a suitable basis for analysing the hyper conjugative or charge transfer interactions and also analysis of inter and intermolecular bonding in molecules or systems. The analysis second order perturbation theory revealed that, the stabilization energy from electron delocalization over the natural bond orbital or hyperconjugation effect is acquired as

$$E^{(2)} = \frac{q_j F(i,j)^2}{\varepsilon_j - \varepsilon_i} \qquad (14)$$

Here, ε_j and ε_i are the energies of i^{th} and j^{th} NBO, named as the acceptor and donor orbitals, respectively for a hyperconjugation. $F(i,j)$ and q_j are the elements of off-diagonal Fock-matrix between i^{th} and j^{th} NBOs and electron population on j^{th} orbital, respectively [84,85]. The enormous estimations of $E^{(2)}$ mirror the presence of more noteworthy interaction between electron-contributors and electron-acceptors, and the degree of conjugation of the whole framework.

Second order interactions obtained by the natural bond orbital analysis are tabulated in Table 6and 7. The π-electron delocalization between these bonds were evident from the $E^{(2)}$ ($E^{(2)}$= 22.53 kcal/mol) values of electron donation from bonding π(C7-C22) orbital to anti-bonding π^*(C8-C25) orbital. There was electron delocalization between the π and π^* orbitals of these bonds reflected by higher value of stabilization energy. We find large hyper-conjugation stabilization ($E^{(2)}$= 43.80 kcal/mol and 30.76 kcal/mol) due to donation of lone pair of O5

(LP(2)) to the π^*(O4-C31) orbital and O4 (LP(2)) to the σ^*(O5-C31) orbital, respectively. This was expected due to resonance effect within the acid group. No significant hyperconjugation involving NBOs with atomic orbitals from Cl is observed except donation from a lone pair of Cl (LP(3)) to π^*(C8-C25) with $E^{(2)}$ = 15.21 kcal/mol, and it comes from small energy difference and a moderate Fock-matrix element value. There are moderate stabilization energies due to electron delocalization within the SO_2NH_2 as shown in the Tables 6 and 7. The title compound have 'push (acid group is capable to push electrons) - pull (chloro group is capable to pull electrons)' groups at para-position and accordingly, making it a potential contender for optical application.

3.10. Sensitivity towards autoxidation

Understanding of degradation path and development of a protocol for the removal of organic pollutants from aquatic media is very essential. Therefore, investigation of lowest H-BDE values is important for the development of new pharmaceutical drugs. This quantity calculation allows the assessment of the possibility of a drug candidate to form degradation products while being stored [86, 87]. Another side was connected to the phase I drug metabolism, during which the carbon-hydrogen bonds were broken for hydroxylation [88, 89]. This underlines the significance of the H-BDE amount to foresee the destiny of the recently combined medications from both ecological and pharmaceutical angles. However, the conduction of these types of studies was a rather tedious task [90, 91], but it could be rationalized and optimized with the of help DFT calculations. Therefore, considering the importance of calculation of H-BDE values, we have performed the calculations and depicted the results in Figure 6.

From the environmental angle [92], as per the earlier literature reports, it can be concluded that the sensitivity towards the autoxidation mechanism was expressed by the H-BDE values that take esteems in a scope of 70–85 kcal/mol. From the analysis of H-BDE values it can be concluded that the title compound could not be sensitive towards autoxidation mechanism due to absence of H-BDE values below 85 kcal/mol. The BDE values have been calculated for all other single acyclic bonds. The title compound has lowest BDE for S-N bond, with BDE value of 54.08 kcal/mol reflecting that degradation could start precisely by breaking of S-N bond.

3.11. Nonlinear Optical (NLO) properties

Figure 7 shows the DFT/CAM-B3LYP/6-311++G(d,p) graphics for the dynamic average linear polarizability and for the linear refractive index as a function of the applied electric field frequency. As it can be seen the $\langle\alpha(-\omega;\omega)\rangle$ values increases monotonically with the

frequency from the static values of $31.1 \times 10^{-24} esu$ to $34.4 \times 10^{-24} esu$ (ω=0.10 a.u.), presenting a percentage increase of 11%. In the same frequency set the linear refractive index goes from 1.62 to 1.70.

The obtained value for the static average second hyperpolarizability was $\langle \gamma(0;0,0,0) \rangle = 23.11 \times 10^{-36} esu$. The dynamic values of the second hyperpolarizabities, corresponding to the dc-Kerr effect and the IDRI process, increases monotonically with the increase of the electric field frequency (Figure 8), reaching the values $\langle \gamma(-\omega;\omega,0,0) \rangle = 39.42 \times 10^{-36} esu$ and $\langle \gamma(-\omega;\omega,\omega,-\omega) \rangle = 55.73 \times 10^{-36} esu$ at $\omega = 0.10\ a.u.$, respectively. Particularly, the values of the second hyperpolarizabilities at the frequency of $\omega = 0.086 a.u.$ (λ=532nm) were $\langle \gamma(-\omega;\omega,0,0) \rangle$ = $33.1 \times 10^{-36} esu$ and $\langle \gamma(-\omega;\omega,\omega,-\omega) \rangle = 43.1 \times 10^{-36} esu$.

Figure 9 shows the DFT/CAM-B3LYP/6-311++G (d, p) results for the third order nonlinear susceptibility as function of the applied electric field frequencies for the BACSBA crystal. In this frequency range, the χ^3 values goes from the static value $\chi^3 = 48.66 \times 10^{-22} m^2/V^2$ to $\chi^3 = 117.2 \times 10^{-22} m^2/V^2$. Table 8 presents some experimental results for organic materials at 532 nm. It can be observed that the χ^3 value for BACSBA was more than five times greater than the experimental results presented in the Table 8 [93]. However, the calculated χ^3 value for BACSBA ($90.68 \times 10^{-22} m^2/V^2$) was nearly 46 times higher than the experimental value obtained for (3Br4MSP) [96] ($1.99 \times 10^{-22} m^2/V^2$). Based on these results, it can be concluded that BACSBA could be investigated for potential use as nonlinear material.

3.12. Thermal analysis

Thermo gravimetric-differential thermal analysis (TG-DTA) spectrum (Figure 10) of BACSBA crystal was recorded on EXSTAR TG/DTA SII 6300 instrument up to 650^{o}C with heating rate 5^{o}C/min in a nitrogen environment. The primary weight loss of 1.1% over the temperature range of 29^{o}C to 234^{o}C was due to elimination of moisture and other volatile materials. The BACSBA crystal faces decomposition in three stages, the first from 235°C to 400°C with major mass loss of 48%. Later, a mass loss of 7 % was observed from 400°C to 500°C, and finally, 44% of mass was lost in the third stage above 650°C. In the TGA graph a sharp endothermic peak was seen at 238°C which reflect the melting of single crystal or phase transition temperature. The shape of the peak indicates the good level of crystallinity of the title compound. From the above thermal analysis, we conclude that the BACSBA crystal is stable up to 234°C without any measurable decomposition. Hence, it may be stated that the title compound is stable and could be used as a NLO material up to 234°C.

3.13. Biological activity studies

(a) Antifungal analysis

The synthesized compound BACSBA was screened for their *in vitro* antifungal activity. The antifungal strains *A.niger* (MTCC-1881), *F.oxysporum* (MTCC-1755) and *A.Foetidus* (NCIM-505) were used and Ketoconazole was used as a standard drug. Zone of inhibition (ZI) was expressed in mm (Table S3). The titled compound BACSBA exhibited promising antifungal activity against all the fungal strains when compared with the standard drug Ketoconazole. This could be due to the presence of sulfonamide moiety present on the benzene ring and other functional groups enhanced the activity.

(b) Antioxidant analysis

Compound BACSBA was evaluated at various concentrations (25, 50, 75, 100 μg/mL) using Butylatedhydroxytoluene (BHT) and Ascorbic acid as standards in DPPH and NO methods (Tables S4 and S5). Compound BACSBA displayed significant activity at all the concentrations in evaluation with the standard drugs. The reason could be the presence of sulfonamide group and other functional groups which improved the antioxidant activity.

4. Conclusion

The SCXRD and optimization of geometry results clearly revealed that the titled compound has an L-shaped structure. Theoretically predicted geometrical parameters and wave numbers were in accordance with the experimental results. HOMO was confined over whole molecule other than amine group, chloro group; while, LUMO was confined over whole molecule other than methyl benzene ring and sulfonamide group. The MESP illustration revealed that the negative potential was affirmed over deprotonated atoms, possible sites for electrophilic attack; the positive potential was affirmed over protonated atoms, possible sites for nucleophilic attack. H-BDE values show that BACSBA molecule was not sensitive towards the autoxidation. However, the titled compound has very low BDE value *i.e.*, 54.08 kcal/mol for the S-N bond, which indicates that degradation could start by breaking of the S2-N24 bond. From the thermal analysis, it might be concluded that the titled compound was stable and can be utilized as NLO material up to 234^{o}C. In the current study, we have used the SM method at DFT/CAM-B3LYP/6-311++G (d,p) level to calculate the electrical parameters such as total dipole moment (μ), the average linear polarization $\langle\alpha(-\omega,\omega)\rangle$ and the second average hyperpolarizability IDRI ($\langle\gamma(-\omega;\omega,\omega,-\omega)\rangle$) for the BACSBA crystal. Optical parameters such as the linear refractive index (n) and the third order nonlinear macroscopic susceptibility ($\chi^3(-\omega;\omega,\omega,\omega)$) of crystal structure BACSBA were calculated. The

examined compound presented better values in the third order macroscopic susceptibility than measured experimental results presented in the literature. The $\chi^{(3)}(-\omega;\omega,\omega,-\omega)$-value of the compound was 5.59 to 45.57 times greatest than the results measured experimentally in the literature. Therefore, the BACSBA crystal has a good suitability for use as a material in applications involving NLO properties. Also, the synthesized molecule displayed most promising antifungal and antioxidant activities. The BACSBA compound exhibited significant antifungal and antioxidant activities compared with the standard drugs. Furthermore, there could be a scope of exploring this class of scaffolds as new and potent antifungal and antioxidant agents which will be a prominent application for medicinal chemists.

Declaration of interests

There was no potential conflict of interest declared by authors.

Acknowledgement

The authors express their grateful thanks to University Grant Commission-Network Resource Center (UGC-NRC), School of Chemistry, University of Hyderabad for providing computational support. Authors also thankful to SAIF, Gauhati University and I.I.T. Madras for the analysis support.

References

[1] N.V. Kamanina, S.V. Serov, N.A. Shurpo, S.V. Likhomanova, D.N. Timonin, P.V. Kuzhakov, N.N. Rozhkova, I.V. Kityk, K.J. Plucinski, D.P. Uskokovic, Polyimide-fullerene nanostructured materials for non-linear optics and solar energy applications, J. Mater. Sci. Mater. Electron. 23 (2012) 1538–1542.

[2] S.V. Likhomanova, N.V. Kamanina, COANP-fullerenes system for optical modulation, J. Phys. Conf. Ser. 741 (2016) 012146.

[3] L. Lu, Z. Liang, L. Wu, Y. Chen, Y. Song, S.C. Dhanabalan, J.S. Ponraj, B. Dong, Y. Xiang, Few-layer Bismuthene : Sonochemical Exfoliation, Nonlinear Optics and Applications for Ultrafast Photonics with Enhanced Stability, Laser Photonics Rev. 12(1) (2017) 1700221.

[4] R. Salvi, C. Cerqueira-coutinho, E. Ricci-junior, N. Santos, S.R. Pinto, E.S. Bernardes, P. Lopes, B. De Araujo, R. Santos-oliveira, R. Salvi, C. Cerqueira-coutinho, E. Ricci-junior, N. Santos, S.R. Pinto, E.S. Bernardes, P. Lopes, Diagnosing lung cancer using etoposide microparticles labeled with ^{99m}Tc, Artificial Cells, Nanomedicine, and Biotechnology An International Journal 48(2) (2018) 341-345.

[5] M. Luo, F. Liang, Y. Song, D. Zhao, F. Xu, N. Ye, Z. Lin, M. Luo, F. Liang, Y. Song, D. Zhao, F. Xu, N. Ye, Z. Lin, $M_2B_{10}O_{14}F_6$ (M = Ca, Sr): Two Noncentrosymmetric Alkaline Earth Fluorooxoborates as Promising Next-Generation Deep-Ultraviolet Nonlinear Optical Materials, J. Am. Chem. Soc. 140(11) (2018) 3884-3887.

[6] H. Zhao, S. Han, R. Hui, Nonlinear Optical Spectroscopy of Two-Dimensional Materials Qiannan Cui, 2017.

[7] G. Shi, Y. Wang, F. Zhang, B. Zhang, Z. Yang, X. Hou, S. Pan, K.R. Poeppelmeier, Finding the Next Deep-Ultraviolet Nonlinear Optical Material: $NH_4B_4O_6F$, J. Am. Chem. Soc. 139 (2017) 10645–10648.

[8] A.N. Castro, L.R. Almeida, M.M. Anjos, G.R. Oliveira, H.B. Napolitano, C. Valverde, B. Baseia, Theoretical study on the third-order nonlinear optical properties and structural characterization of 3-Acetyl-6-Bromocoumarin, Chem. Phys. Lett. 653 (2016) 122–130.

[9] M. Boztaş, Y. Çetinkaya, M. Topal, Synthesis and carbonic anhydrase isoenzymes I, II, IX, and XII inhibitory effects of dimethoxy-bromophenol derivatives incorporating cyclopropane moieties, J. Med. Chem. 58(2) (2015) 640-650.

[10] Y. Akbaba, A. Akıncıoğlu, H. Göçer, Carbonic anhydrase inhibitory properties of novel sulfonamide derivatives of aminoindanes and aminotetralins, J. Enzyme Inhib. Med. Chem. 29(1) (2014) 35-42.

[11] H.İ. Gül, K. Kucukoglu, C. Yamali, Synthesis of 4-(2-substitutedhydrazinyl) benzenesulfonamides and their carbonic anhydrase inhibitory effects, J. Enzyme Inhib. Med. Chem. 31(4) (2016) 568-573.

[12] H.İ. Gül, M. Tuğrak, H. Sakagami, Synthesis and bioactivity studies on new 4-(3-(4-substituted phenyl)-3a,4-dihydro-3*H*-indeno[1,2-c]pyrazol-2-yl) benzene sulfonamides, J. Enzyme Inhib. Med. Chem. 31(6) (2016) 1619-1624.

[13] B. Thirumalaiselvam, R. Kanagadurai, D. Jayaraman, V. Natarajan, Growth and characterization of 4-methyl benzene sulfonamide single crystals, Optical Materials 37 (2014) 74-79.

[14] N. Hirayama, J. Taga, S. Oshima, T. Honjo, Sulfonamide-type di-schiff base ligands as chelate extraction reagents for divalent metal cations, Anal. Chim. Acta 466 (2002) 295-301.

[15] Par J. Lamotre, H. Campsteyn, L.D.M. Vermeire, Crystal and Molecular Structure of Furfurylamino-2-Chloro-4-Sulfamoyl-5-Acid ($C_{12}H_{II}ClN_2O_5S$), Acta Cryst. B34 (1978) 1657-1661.

[16] N. Jagadeesh Babu, S. Cherukuvada, Ranjit Thakuria, Ashwini Nangia, Conformational and Synthon Polymorphism in Furosemide (Lasix), Crystal Growth & Design 10(4) (2010) 1979-1989.

[17] Olcay Bolukbasi, Ayberk Yilmaz, X-ray structure analysis and vibrational spectra of Furosemide, Vib. Spectrosc. 62 (2012) 42-49.

[18] Alastair Florence, Andrea Johnston, Philippe Fernandes, Kenneth Shankland, Howard N.E. Stevens, Sigrunn Osmundsen, Alexander B. Mullen, Powder study of hydrochlorothiazide form II, Acta Cryst. E61 (2005) o2798-o2800.

[19] Juan M. Aceves-Hernández, Esther Agacino-Valdés, Manuel Paz, Jaime Hinojosa-Torres, Experimental and theoretical study of the conformational analysis of hydrochlorothiazide, J. Mol. Struct. 786 (2006) 1-8.

[20] Andrea Johnston, Alastair J. Florence, Alan R. Kennedy, Hydrochlorothiazide *N*,*N*-dimethylformamide solvate, Acta Cryst. E62 (2006) o1730–o1732

[21] Philippe Fernandes, Alastair J. Florence, Kenneth Shankland, Norman Shankland, Andrea Johnston, Powder study of chlorothiazide *N*,*N*-dimethylformamide solvate, Acta Cryst. E62 (2006) o2216–o2218.

[22] M. Boopathi, P. Udhayakal, T.V. Rajendiran, Theoretical calculation of molecular structure, vibrational spectra, and molecular electrostatic potential of metolazone, J Appl Spectrosc. 83(1) (2016) 12-19.

[23] E.E. Porchelvi, S. Muthu, The spectroscopic (FT-IR, FT-Raman and NMR), NCA, Fukui function analysis first order hyperpolarizability, TGA of 6-chloro-3,4-dihydro-2*H*-1,2,4-benzothiazine-7-sulphonamide1,1-dioxide by ab initio HF and Density Functional method, Spectrochim. Acta 123 (2014) 230–240.

[24] Ch. Kavitha, K. Narendra, A. Ratnakar, N. Poojith, C. Sampath, Subrata Banik, P.A. Suchetan, Krishna Murthy Potla, N. Venkatasubba Naidu, An analysis of structural, spectroscopic signatures, reactivity and anti-bacterial study of synthetized 4-chloro-3-sulfamoylbenzoic acid, J. Mol. Struct. 1202 (2020) 127176.

[25] Mujeeb Ur Rahman, Ankita Rathore, Anees A. Siddiqui, Gazala Parveen, M. Shahar Yar, Synthesis and characterization of quinazoline derivatives: search for hybrid molecule as diuretic and antihypertensive agents, J. Enzyme Inhib. Med. Chem. 29(5) (2014) 733-743.

[26] P. Krishna Murthy, C. Valverde, V. Suneetha, Stevan Armaković, Sanja J. Armaković, N. Usha Rani, N. Venkatasubba Naidu, An analysis of structural and spectroscopic signatures, the reactivity study of synthetized 4,6-dichloro-2-

(methylsulfonyl)pyrimidine: A potential third-order nonlinear optical material, J. Mol. Struct.1186 (2019) 263-275.

[27] P. Krishna Murthy, V. Suneetha, Stevan Armaković, Sanja J. Armaković, C. Van Alsenoy, P.A. Suchetan, R. Sreenivasa Rao, Synthesis, characterization and computational study of the newly synthetized sulfonamide molecule, J. Mol. Struct. 1153 (2018) 212-229.

[28] Bruker APEX2, SADABS, SAINT-Plus and XPREP Bruker AXS Inc., Madison, Wisconsin, USA2009.

[29] G.M. Sheldrick, A short history of SHELX, ActaCryst. A64 (2008) 112-122.

[30] K. Burke, Perspective on density functional theory, J. Chem. Phys. 136 (2012) 150901.

[31] Gaussian 09, Revision B.01, M.J. Frisch, G.W. Trucks, H.B. Schlegel, G.E. Scuseria, M.A. Robb, J.R. Cheeseman, G. Scalmani, V. Barone, B. Mennucci, G.A. Petersson, H. Nakatsuji, M. Caricato, X. Li, H.P. Hratchian, A.F. Izmaylov, J. Bloino, G. Zheng, J.L. Sonnenberg, M. Hada, M. Ehara, K. Toyota, R. Fukuda, J. Hasegawa, M. Ishida, T. Nakajima, Y. Honda, O. Kitao, H. Nakai, T. Vreven, J.A. Montgomery, J.E. Peralta, F. Ogliaro, M. Bearpark, J.J. Heyd, E. Brothers, K.N. Kudin, V.N. Staroverov, T. Keith, R. Kobayashi, J. Normand, K. Raghavachari, A. Rendell, J.C. Burant, S.S. Iyengar, J. Tomasi, M. Cossi, N. Rega, J.M. Millam, M. Klene, J.E. Knox, J.B. Cross, V. Bakken, C. Adamo, J. Jaramillo, R. Gomperts, R.E. Stratmann, O. Yazyev, A.J. Austin, R. Cammi, C. Pomelli, J.W. Ochterski, R.L. Martin, K. Morokuma, V.G. Zakrzewski, G.A. Voth, P. Salvador, J.J. Dannenberg, S. Dapprich, A.D. Daniels, O. Farkas, J.B. Foresman, J.V. Ortiz, J. Cioslowski, D.J. Fox, Gaussian, Inc., Wallingford CT, 2010.

[32] Michal H. Jamroz, Vibrational Energy Distribution Analysis VEDA4, Warsaw, 2004-2010.

[33] J.B. Foresman, Pittsburg, PA, in: E. Frisch (Ed.), Exploring Chemistry with Electronic Structure Methods: a Guide to Using Gaussian, 1996.

[34] Tian Lu, Feiwu Chen, Multiwfn: A multifunctional wavefunction analyzer, J. Comput. Chem. 33 (2012) 580-592.

[35] C. Valverde, F.A.P. Osório, T.L. Fonseca, B. Baseia, DFT study of third-order nonlinear susceptibility of a chalcone crystal, Chem. Phys. Lett. 706 (2018) 170–174.

[36] J.M.F. Custodio, G.D.C. D'Oliveira, F. Gotardo, L.H.Z. Cocca, L. De Boni, C.N. Perez, L.J.Q. Maia, C. Valverde, F.A.P. Osório, H.B. Napolitano, Chalcone as

Potential Nonlinear Optical Material: A Combined Theoretical, Structural, and Spectroscopic Study, J. Phys. Chem. C 123 (2019) 5931–5941.

[37] J.M.F. Custodio, R.R. Ternavisk, C.J.S. Ferreira, A.S. Figueredo, G.L.B. Aquino, H.B. Napolitano, C. Valverde, B. Baseia, Using the Supermolecule Approach To Predict the Nonlinear Optics Potential of a Novel Asymmetric Azine, J. Phys. Chem. A 123 (2019) 153–162.

[38] T.L. Fonseca, J.R. Sabino, M.A. Castro, H.C. Georg, A theoretical investigation of electric properties of L-arginine phosphate monohydrate including environment polarization effects, J. Chem. Phys. 133 (2010) 1–8.

[39] O.L. Santos, T.L. Fonseca, J.R. Sabino, H.C. Georg, M.A. Castro, Polarization effects on the electric properties of urea and thiourea molecules in solid phase, J. Chem. Phys. 143 (2015) 234503.

[40] R.F.W. Bader, A quantum theory of molecular structure and its applications, Chem. Rev. 91 (1991) 893–928.

[41] R.F.W. Bader, Atoms in molecules, Acc. Chem. Res. 18 (1985) 9–15.

[42] R.F.W. Bader, Atoms in molecules : A quantum theory, Clarendon Press, 1990.

[43] B. Galdino, D. Oliveira, R. De Cássia, M. Ugulino, D. Araújo, Full Paper Uma comprovação químico-quântica sobre a formação de ligações de hidrogênio e interações secundárias em sistemas heterocíclicos intermoleculares Introdução, 1 (2009) 167–182.

[44] R.F.W. Bader, The quantum mechanical basis of conceptual chemistry, Monatshefte für Chemie / Chemical Monthly, 136 (2005) 819–854.

[45] M. Burits, F. Bucar, Antioxidant activity of Nigella sativa essential oil, Phytother. Res. 14(5) (2000) 323-328.

[46] M. Cuendet, K. Hostettmann, O.P. Otterat, Iridoid Glucosides with Free Radical Scavenging Properties from Fagraea blumei, Helv. Chim. Acta. 80(4) (1997) 1144-1152.

[47] K. Kato, S. Terao, N. Shimamoto, M. Hirata, Studies on scavengers of active oxygen species. 1. Synthesis and biological activity of 2-O-alkylascorbic acids, J. Med. Chem. 31(4) (1988) 793-798.

[48] L. Marcocci, L. Packer, M.T. Droy-Lefaix, A. Sekaki, M. Gardes-Albert, Antioxidant action of Ginkgo biloba extract EGb 761, Methods Enzymol. 234 (1994) 462-75.

[49] I. Rozas, I. Alkorta, J. Elguero, Behavior of Ylides Containing N, O, and C Atoms as Hydrogen Bond Acceptors, J. Am. Chem. Soc. 122 (2000) 11154–11161.

[50] Mark A. Spackman, Dylan Jayatilaka, Hirshfeld surface analysis, CrystEngComm. 11 (2009) 19-32.

[51] F.L. Hirshfeld, Bonded-Atom Fragments for Describing Molecular Charge Densities, Theor. Chim. Acta 44 (1977) 129-138.

[52] H.F. Clausen, M.S. Chevallier, M.A. Spackman, B.B. Iversen, Three new co-crystals of hydroquinone: crystal structures and Hirshfeld surface analysis of intermolecular interactions, New J. Chem. 34 (2010) 193-199.

[53] A.L. Rohl, M. Moret, W. Kaminsky, K. Claborn, J.J. McKinnon, B. Kahr, Hirshfeld surfaces identify inadequacies in computations of intermolecular interactions in crystals: pentamorphic 1, 8-dihydroxyanthraquinone, Cryst. Growth Des. 8 (2008) 4517-4525.

[54] A. Parkin, G. Barr, W. Dong, C.J. Gilmore, D. Jayatilaka, J.J. McKinnon, M.A. Spackman, C.C. Wilson, Comparing entire crystal structures: structural genetic fingerprinting, CrystEngComm. 9 (2007) 648-652.

[55] M.A. Spackman, J.J. McKinnon, Fingerprinting intermolecular interactions in molecular crystals, CrystEngComm. 4 (2002) 378-392.

[56] S.K. Wolff, D.J. Grimwood, J.J. McKinnon, D. Jayatilaka, M.A. Spackman, Crystal Explorer 2.0; University of Western Australia, Australia, 2012.

[57] K. Tamagawa, T. Iijima, M. Kimura, Molecular structure of benzene, J. Mol. Struct. 30 (1976) 243-253.

[58] J. Lukose, C.Y. Panicker, P.S. Nayak, B. Narayana, B.K. Sarojini, C. Van Alsenoy, A.A. Al-Saadi, Synthesis, structural and vibration investigation of 2-phenyl-N-(pyrazin-2-yl)acetamide combining XRD diffraction, FT-IR and NMR spectroscopies with DFT calculations, Spectrochim. Acta 135 (2015) 608-616.

[59] P. Krishna Murthy, Y. Sheena Mary, Y. Shyma Mary, C.Y. Panicker, V. Suneetha, Stevan Armaković, Sanja J. Armaković, C. Van Alsenoy, P.A. Suchetan, Synthesis, crystal structure analysis, spectral investigations, DFT computations and molecular dynamics and docking study of 4-benzyl-5-oxomorpholine-3-carbamide, a potential bioactive agent, J. Mol. Struct. 1134 (2017) 25-39.

[60] P. Krishna Murthy, G. Krishna Swamy, Stevan Armaković, Sanja J. Armaković, P.A. Suchetan, Nivedita R Desai, V. Suneetha, R. Sreenivasa Rao, G. Bhargavi, D.B. Aruna Kumar, Structural and spectroscopic characterization, reactivity study and charge transfer analysis of the newly synthetized 2-(6-hydroxy-1-benzofuran-3-yl) acetic acid, J. Mol. Struct. 1162 (2018) 81-95.

[61] N.P.G. Roeges, A guide to the complete interpretation of IR spectra of Organic Compounds, Wiley, New York, 1994.

[62] N.B. Colthup, L.H. Daly, S.E. Wiberly, Introduction to IR and Raman Spectroscopy, Academic Press, New York, 1990.

[63] R.M. Silverstein, G.C. Bassler, T.C. Morril, Spectrometric Identification of Organic Compounds, fifth ed., John Wiley and Sons Inc., Singapore, 1991.

[64] L.J. Bellamy, The Infrared Spectrum of Complex Molecules, third ed., Chapman and Hall, London, 1975.

[65] S. Beegum, Y.S. Mary, H.T. Varghese, C.Y. Panicker, Stevan Armaković, Sanja J. Armaković, J. Zitko, M. Dolezal, C. Van Alsenoy, Vibrational Analysis of cyanopyrazine-2-carboxamide derivatives and investigation of their reactive properties by DFT calculations and molecular dynamic simulations, J. Mol. Struct. 1131 (2017) 1-15.

[66] G. Louran, M. Lapkowski, S. Quillard, A. Pron, J.B. Buisson, S. Lefrant, Vibrational Properties of Polyaniline-Isotope Effects, J. Phys. Chem. 100 (1996) 6998.

[67] Tintu K. Kuruvilla, Johanan Christian Prasana, S. Muthu, Jacob George, Sheril Ann Mathew, Quantum mechanical and spectroscopic (FT-IR, FT-Raman) study, NBO analysis, HOMO-LUMO, first order hyperpolarizability and molecular docking study of methyl [(3R)-3-(2-methylphenoxy)-3-phenylpropyl]amine by density functional method, Spectrochim. Acta 188 (2018) 382-393.

[68] R.J. Parr, L.V. Szentpaly, S. Liu, Electrophilicity index, J. Am. Chem. Soc. 121 (1999) 1922-1924.

[69] A. Kumar, S.R. Gadre, N. Mohan, C.H. Suresh, Lone Pairs: An Electrostatic View point, J. Phys.Chem. A 118 (2014) 526–532.

[70] S.R. Gadre, S.S. Pundlik, Complementary Electrostatics for the Study of DNA Base-Pair Interactions, J. Phys. Chem. B 101 (1997) 3298–3303.

[71] P. Politzer, D.G. Truhlar, in Chemical Application of Atomic and Molecular Electrostatic Potential, Springer, New York, 4 (1981) 472.

[72] P. Sjoberg, P. Politzer, Use of the electrostatic potential at the molecular surface to interpret and predict nucleophilic processes, J. Phys. Chem. 94 (1990) 3959–3961.

[73] I. Sidir, Y.G. Sidir, M. Kumalar, E. Tasal, Ab initio Hartree-Fock and density functional theory investigations on the conformational stability, molecular structure and vibrational spectra of 7-acetoxy-6-(2,3-dibromopropyl)-4,8-dimethylcoumarin molecule, J. Mol. Struct. 964 (2010) 134-138.

[74] V. Balachandran, K. Parimala, Tautomeric purine forms of 2-amino-6-chloropurine (N_9H_{10} and N_7H_{10}): structures, vibrational assignments, NBO analysis, hyperpolarizability, HOMO-LUMO study using B3 based density functional calculations, Spectrochim. Acta 96 (2012) 340-351.

[75] A. Lakshmi, V. Balachandran, Rotational isomers, NBO and spectral analyses of N-(2-hydroxyethyl) phthalimide based on quantum chemical calculations, J. Mol. Struct. 1033 (2013) 40-50.

[76] S. Ramalingama, M. Karabacak, S. Periandy, N. Puviarasan, D. Tanuja, Spectroscopic (infrared, Raman, UV and NMR) analysis, Gaussian hybrid computational investigation (MEP maps/HOMO and LUMO) on cyclohexanoneoxime, Spectrochim. Acta 96 (2012) 207-212.

[77] P. Kolandaivel, G. Praveen, P. Selvarengan, Study of atomic and condensed atomic indices for reactive sites of molecules, J. Chem. Sci. 117 (2005) 591-598.

[78] A.D. Becke, K.E. Edgecombe, A simple measure of electron localization in atomic and molecular systems, J. Chem. Phys. 92 (1990) 5397-5403.

[79] Christina Susan Abraham, Johanan Christian Prasana, S. Muthu, B. Fathima Rizwana, M. Raja, Quantum computational studies, spectroscopic (FT-IR, FT Raman and UV-Vis) profiling, natural hybrid orbital and molecular docking analysis on 2,4 Dibromoaniline, J. Mol. Struct.1160 (2018) 393-405.

[80] Jordi Poater, Miquel Duran, Miquel Solà, Bernard Silvi, Theoretical evaluation of electron delocalization in aromatic molecules by means of atoms in molecules (AIM) and electron Localization function (ELF) topological approaches, Chem. Rev. 105 (2005) 3911-3947.

[81] Tintu K. Kuruvilla, S. Muthu, Johanan Christian Prasana, Jacob George, S. Sevvanthi, Spectroscopic (FT-IR, FT-Raman), quantum mechanical and docking studies on methyl[(3S)-3-(naphthalen-1-yloxy)-3-(thiophen-2-yl) propyl]amine, J. Mol. Struct. 1175 (2019) 163-174.

[82] B. Fathima Rizwana, S. Muthu, Johanan Christian Prasana, Christina, Susan Abraham, M. Raja, Spectroscopic (FT-IR,FT-Raman) investigation, topology (ESP,ELF,LOL) analyses, charge transfer excitation and molecular docking (dengue, HCV) studies on ribavirin, Chem. Data Collect. 17-18 (2018) 236-250.

[83] E.D. Glendening A.E. Reed, J.E. Carpenter, F. Weinhold, NBO Version 3.1, Gaussian Inc., Pittsburgh, PA, 2003.

[84] E.D. Glendening, C.R. Landis, F. Weinhold, Natural bond method, Wires computational molecular science 2 (2012) 1-42.

[85] M.N. Tahir, M. Khalid, A. Islam, S.M.A. Mashhadi, A.A.C. Braga, Facile synthesis, single crystal analysis, and computational studies of sulphanilamide derivatives, J. Mol. Struct. 1127 (2017), 766-776.

[86] T. Andersson, A. Broo, E. Evertsson, Prediction of Drug Candidates' Sensitivity Toward Autoxidation: Computational Estimation of C-H Dissociation Energies of Carbon□Centered Radicals, J. Pharm. Sci. 103 (2014) 1949–1955.

[87] P. Lienard, J. Gavartin, G. Boccardi, M. Meunier, Predicting drug substances autoxidation, Pharm. Res. 32 (2015) 300–310.

[88] K.L.M. Drew, J. Reynisson, The impact of carbon–hydrogen bond dissociation energies on the prediction of the cytochrome P450 mediated major metabolic site of drug-like compounds, Eur. J. Med. Chem. 56 (2012) 48–55.

[89] P.R. Ortiz de Montellano, Hydrocarbon hydroxylation by cytochrome P450 enzymes, Chem. Rev. 110 (2009) 932–948.

[90] S. Klick, P.G. Muijselaar, J. Waterval, T. Eichinger, C. Korn, T.K. Gerding, A.J. Debets, C. Sänger-van de Griend, C. van den Beld, G.W. Somsen, Stress testing of drug substances and drug products, Pharm. Technol. 29 (2005) 48–66.

[91] K.M. Alsante, L. Martin, S.W. Baertschi, A stress testing bench marking study, Pharm. Technol. 27 (2003) 60–73.

[92] J.S. Wright, H. Shadnia, L.L. Chepelev, Stability of carbon□centered radicals: Effect of functional groups on the energetics of addition of molecular oxygen, J. Comput. Chem. 30 (2009) 1016–1026.

[93] A.N. Prabhu, V. Upadhyaya, A. Jayarama, K.S. Bhat, Third-order NLO property of thienyl chalcone derivative: Physicochemical analysis and crystal structure determination, Mol. Cryst. Liq. Cryst. 637 (2016) 76–86.

[94] K. Naseema, K. Sujith, K.B. Manjunatha, B. Kalluraya, G. Umesh, V. Rao, Synthesis, characterization and studies on the nonlinear optical parameters of hydrazones, Opt. Laser Technol. 42 (2010) 741–748.

[95] H.J. Ravindra, K. Chandrashekaran, W.T.A. Harrison, S.M. Dharmaprakash, Structure and NLO property relationship in a novel chalcone co-crystal, Appl. Phys. B. 94 (2009) 503–511.

[96] E.D. D'silva, G.K. Podagatlapalli, S. Venugopal Rao, S.M. Dharmaprakash, Study on third-order nonlinear optical properties of 4-methylsulfanyl chalcone derivatives using picosecond pulses, Mater. Res. Bull. 47 (2012) 3552–3557.

Figures

Scheme -1: Synthetic scheme for 2-(benzylamino)-4-chloro-5-sulfamoylbenzoic acid (BACSBA).

Figure 1. Some potent biologically active chlorosulfonamide drug moieties.

Figure 2. ORTEP view of 2-(benzylamino)-4-chloro-5-sulfamoylbenzoic acid (BACSBA) with thermal ellipsoids drawn at 50% probability.

Figure 3. Packing of molecules in the crystal lattice of BACSBA.

Figure 4. Dipole moment values as function of the iterative steps.

Figure 5. Analysis of 3D-Hirshfeld surfaces and 2D-finger print plots of BACSBA molecule.

Figure 6. H-BDE (violet color) and BDE (green color) values for BACSBA molecule.

Figure 7. Linear polarizability and linear refractive index as function of the electric field frequencies

Figure 8. Second hyperpolarizabilities $\langle\gamma(-\omega;\omega,0,0)\rangle$ and $\langle\gamma(-\omega;\omega,\omega,-\omega)\rangle$ ($in\ units\ of\ 10^{-36}esu$) as function of the electric field frequencies.

Figure 9. Third-order nonlinear susceptibility ($10^{-22}m^2/V^2$) as function of the frequency.

Figure 10. DTA/TGA graph of BACSBA compound.

Tables

Table 1. Crystal data and structure refinement for BACSBA.

Table 2. Geometric parameters for hydrogen bonds (A, °) operating in the crystal structure of BACSBA.

Table 3. Topological analysis performed *via* QTAIM, all data are in a.u.

Supplementary Information

Table 1.

Crystal data and structure refinement for BACSBA.

CCDC No.	1920200
Empirical formula	$C_{14}H_{13}N_2O_4SCl$
Formula weight	340.77
Temperature/K	296.15
Crystal system	monoclinic
Space group	*C*2/*c*
a/Å	18.8442(12)
b/Å	5.2862(3)
c/Å	30.4756(19)
α/°	90
β/°	101.800(6)
γ/°	90
Volume/Å^3	2971.6(3)
Z	8
ρ_{calc}g/cm^3	1.523
μ/mm^{-1}	0.417
F(000)	1408.0
Crystal size/mm^3	0.25 × 0.22 × 0.18
Radiation	MoKα (λ = 0.71073)
2Θ range for data collection/°	4.416 to 60.384
Index ranges	$-26 \leq h \leq 26$, $-7 \leq k \leq 7$, $-42 \leq l \leq 42$
Reflections collected	30020
Independent reflections	4356 [R_{int} = 0.0399, R_{sigma} = 0.0255]
Data/restraints/parameters	4356/2/215
Goodness-of-fit on F^2	1.140
Final R indexes [I>=2σ (I)]	R_1 = 0.0480, wR_2 = 0.1273
Final R indexes [all data]	R_1 = 0.0605, wR_2 = 0.1357
Largest diff. peak/hole / e Å^{-3}	0.32/-0.55

Table 2.

Geometric parameters for hydrogen bonds (A, °) operating in the crystal structure of BACSBA.

D-H…A	D-H	H…A	D…A	D-H…A
N19-H33...O4[#]	0.83	2.03	2.7120	139
O5-H32...O4[i]	0.81	1.83	2.6391	176
N24-H34...O3[ii]	0.85	2.14	2.9216	153
N24-H35...O3[iii]	0.80	2.36	3.1234	161

[#]Intra; i: 1-x,3-y,-z; ii: x,1+y,z; iii: 1/2-x,3/2-y,-z

Table 3.
Topological analysis performed *via* QTAIM, all data are in a.u..

BCP	$\rho(r_{bcp})$	$\nabla^2\rho(r_{bcp})$	$V(r_{bcp})$	$G(r_{bcp})$	$H(r_{bcp})$	Interactions
1	0.02931	0.1104	-0.02330	0.02546	0.00215	N19–H33···O4
2	0.05165	0.1431	-0.05052	0.04315	0.00736	O5–H32···O4
3	0.02119	0.0877	-0.01588	0.01891	0.00302	N24–H34···O3
4	119.576	-544471	-136133	7.86953	-136125	N24–H35···O3

Table 4.

Geometrical parameters of the title compound.

Bond length (Å) DFT/XRD			
C31-O4	1.22146/1.232	C31-O5	1.35789/1.307
C20-N19	1.35620/1.346	C16-N19	1.45343/1.445
C31-C21	1.46570/1.465	C21-C22	1.40125/1.389
C22-C7	1.38215/1.383	C7-C8	1.41065/1.409
C8-C25	1.37954/1.368	C25-C20	1.41468/1.417
C20-C21	1.43036/1.426	C8-Cl1	1.74327/1.7295
C15-C13	1.39773/1.390	C13-C11	1.39356/1.389
C11-C9	1.39365/1.356	C27-C9	1.39383/1.360
C27-C29	1.39373/1.393	C29-C15	1.39655/1.377
S2-O3	1.45602/1.4448	C7-S2	1.81239/1.7565
S2-O6	1.45595/1.4211	S2-N34	1.66250/1.5978
Bond angle (º) DFT/XRD			
O3-S2-O6	122.25743/118.53	C7-S2-N24	106.62024/107.80
O3-S2-N24	105.76817/105.91	O6-S2-N24	105.73479/108.06
C7-S2-O3	107.69232/107.00	C7-S2-O6	107.82117/109.08
O4-C31-O5	120.33229/122.01	C20-N19-C16	125.24333/124.12
C21-C31-O4	125.72039/123.25	C21-C31-O5	113.94732/114.74
C21-C20-N19	121.58549/122.40	C25-C20-N19	120.90577/120.45
C7-C8-Cl1	121.33440/120.77	C7-C8-C25	121.12101/121.51
C25-C8-Cl1	117.54416/117.72	C8-C7-C22	117.86587/117.50
C7-C22-C21	122.65573/122.57	C22-C21-C20	119.31128/119.80
C21-C20-C25	117.50866/117.15	C20-C25-C8	121.53339/121.44
C29-C15-C13	118.92514/118.1	C15-C16-N19	115.69221/115.15
C9-C27-C29	120.26841/120.3	C13-C11-C9	120.04183/120.3
C27-C29-C15	120.48045/120.6		
Torsion angle (º) DFT/XRD			
O3-S2-C7-C22	113.31709/105.43	O3-S2-C7-C8	-66.70601/-74.19
O6-S2-C7-C22	-112.97318/-125.21	O6-S2-C7-C8	67.00371/55.17
24N-S2-C7-C22	0.18254/-8.10	N24-S2-C7-C8	-179.84056/172.28
O4-C31-C21-C20	0.05405/0.7	O4-C31-C21-C22	-179.62284/179.37
O5-C31-C21-C20	-179.95423/-178.86	O5-C31-C21-C22	0.36889/-0.2
C21-C20-N19-C16	-175.82528/-179.43	C25-C20-N19-C16	4.06980/0.9
C29-C15-C16-N19	-30.51518/-11.6	C13-C15-C16-N19	151.80849/169.8

Table 5.

Fukui Condensed Functions are evaluated by Frontier Molecular Orbital Method for BACSBA.

Atoms	Atomic No.	HOMO electrophilic attack	LUMO Nucleophilic attack	Radical attack	Dual-Descriptor	Hardness	Local electrophilic	Local Nucleophilic
N	Z	f_r-	f_k+	f_k0	Δf_r	(au)	W-(eV)	W+(eV)
Cl1	17	0.0004	0.0304	0.0154	0.0300	-0.0022	0.0009	0.0636
S2	16	0.0011	0.0013	0.0012	0.0002	0.0002	0.0024	0.0028
O3	8	0.0327	0.0005	0.0166	-0.0322	0.0077	0.0685	0.0011
O4	8	0.0236	0.1280	0.0758	0.1043	-0.0042	0.0495	0.2678
O5	8	0.0087	0.0438	0.0263	0.0351	-0.0013	0.0182	0.0917
O6	8	0.0326	0.0005	0.0166	-0.0321	0.0077	0.0682	0.0011
C7	6	0.1574	0.0000	0.0787	-0.1573	0.0374	0.3294	0.0001
C8	6	0.0013	0.2040	0.1027	0.2028	-0.0154	0.0027	0.4271
C9	6	0.0013	0.0005	0.0009	0.2028	0.0003	0.0026	0.0010
C11	6	0.0012	0.0002	0.0007	-0.0010	0.0003	0.0025	0.0004
C13	6	0.0042	0.0010	0.0026	-0.0033	0.0009	0.0089	0.0020
C15	6	0.0521	0.0071	0.0296	-0.0450	0.0118	0.1091	0.0149
C16	6	0.0035	0.0035	0.0035	0.0000	0.0006	0.0073	0.0072
N19	7	0.3633	0.0311	0.1972	-0.3322	0.0840	0.7603	0.0650
C20	6	0.0270	0.0670	0.0470	0.0400	0.0013	0.0565	0.1402
C21	6	0.1296	0.0949	0.1122	-0.0347	0.0235	0.2712	0.1987
C22	6	0.0150	0.1451	0.0801	0.1301	-0.0076	0.0315	0.3037
N24	7	0.0002	0.0009	0.0005	0.0007	0.0000	0.0004	0.0018
C25	6	0.1069	0.0696	0.0883	-0.0373	0.0201	0.2238	0.1457
C27	6	0.0005	0.0008	0.0007	0.0004	0.0001	0.0010	0.0018
C29	6	0.0051	0.0012	0.0031	-0.0039	0.0011	0.0107	0.0025
C31	6	0.0056	0.1595	0.0826	0.1539	-0.0109	0.0118	0.3339

Table 6.
Second-order perturbation theory analysis of Fock matrix in NBO basis corresponding to the intramolecular bonds of the title compound.

Donor(i)	Type	ED/e	Acceptor(j)	Type	ED/e	E(2)[a]	E(j)-E(i)[b]	F(i,j)[c]
C7-C22	π	1.73363	C8-C25	π*	0.02632	22.53	0.29	0.074
C8-C25	π	1.73601	C7-C22	σ*	0.02357	13.08	0.29	0.057
C8-C25	π	1.73601	C7-C22	π*	0.35856	13.08	0.29	0.057
LP Cl1	3	1.90376	C8-C25	π*	0.34483	15.21	0.32	0.067
LP O3	π	1.81211	S2-C7	σ*	0.21524	18.15	0.42	0.078
LP O3	3	1.77677	S2-O6	σ*	0.14452	17.90	0.59	0.093
			S2-N24	σ*	0.22437	15.48	0.42	0.072
LP O4	π	1.85075	O5-C31	σ*	0.08862	30.76	0.62	0.125
-	-		C21-C31	σ*	0.05781	14.90	0.72	0.094
LP O5	π	1.83108	O4-C31	π*	0.29690	43.80	0.34	0.112
LP O6	π	1.81194	S2-C7	σ*	0.21524	18.20	0.42	0.079
LP O6	3	1.77683	S2-O3	σ*	0.14471	17.93	0.59	0.093
			S2-N24	σ*	0.22437	15.47	0.42	0.072

[a] E(2) means energy of hyper-conjugative interactions (stabilization energy in kcal/mol)
[b] Energy difference (a.u) between donor and acceptor i and j NBO orbitals
[c] F(i,j) is the Fock matrix elements (a.u) between i and j NBO orbitals

Table 7.

NBO results showing the formation of Lewis and non-Lewis orbitals.

Bond(A-B)	ED/e[a]	EDA%	EDB%	NBO	s%	p%
n1 S2-O3	1.98830	35.88	64.12	0.5990(SP2.55)S+	27.75	70.67
-	-0.99195	-	-	0.8007(SP3.13)O	24.16	75.70
n1 S2-O6	1.98832	35.89	64.11	0.5991(SP2.55)S+	27.76	70.67
-	-0.99205	-	-	0.8007(SP3.13)O	24.16	75.70
n1 S2-C7	1.96753	47.20	52.80	0.6870(SP3.09)S+	24.07	74.39
-	-0.68730	-	-	0.7267(SP3.26)O	23.47	76.47
n1 S2-N24	1.98492	37.18	62.82	0.6098(SP3.75)S+	20.65	77.42
-	-0.81430	-	-	0.7926(SP2.50)N	28.57	71.36
n2 O4-C31	1.99477	65.48	34.52	0.8092(SP1.45)O+	40.75	59.13
-	-1.09505	-	-	0.5875(SP2.03)C	32.93	66.93
n1 O5-C31	1.99464	68.50	31.50	0.8276(SP1.92)O+	34.17	1.92
-	-0.95544	-	-	0.5613(SP2.76)C	26.52	73.24
n2 C7-C22	1.73363	58.19	41.81	0.7628(SP1.00)C+	0.00	99.98
-	-0.29407	-	-	0.6466(SP1.00)C	0.00	99.94
n2 C8-C25	1.73601	47.70	52.30	0.6906(SP1.00)C+	0.00	99.96
-	-0.29610	-	-	0.7232(SP1.00)C	0.00	99.95
n1 C21-C31	1.97497	52.04	47.96	0.7214(SP2.29)C+	30.40	69.55
-	-0.70296	-	-	0.6925(SP1.48)C	4.38	59.58
n1 O4-C31	1.99477	65.48	34.52	0.8092(SP1.45)O+	40.75	59.13
-	-1.09505	-	-	0.5875(SP2.03)C	32.93	66.93
n2 O4-C31	1.98406	71.68	28.32	0.8466(SP1.00)O+	0.00	99.89
-	-0.40916	-	-	0.5322(SP1.00)C	0.00	99.46
n2 C8-C25	1.73601	47.70	52.30	0.6906(SP1.00)C+	0.00	99.96
-	-0.29610	-	-	0.7232(SP1.00)C	0.00	99.95
n3Cl	1.90376	-	-	sp1.00	0.00	99.96
-	-0.32536	-	-	-	-	-
n2 O3	1.81211	-	-	sp1.00	0.00	99.92
	-0.29020					
n3 O3	1.77677	-	-	sp99.99	0.04	99.88
	-0.28923					
n2 O4	1.85075	-	-	sp99.99	0.17	99.77
	-0.30029					
n2 O5	1.83108	-	-	sp1.00	0.00	99.94
	-0.35845					
n2 O6	1.81194	-	-	sp1.00	0.00	99.92
	-0.29010					
n3 O6	1.77683	-	-	sp99.99	0.04	99.88
	-0.28916					
n1 C21	1.15180	-	-	sp1.00	0.00	100
	-0.14469					

[a] ED/e is expressed in a.u.

Table 8.
Third-order nonlinear optical susceptibility value for BACSBA crystal compared with experimental results of organic crystals.

Crystals	$\chi^{(3)}\left(10^{-22}\left(\frac{m}{V}\right)^2\right)$
BACSBA (present work)	90.68
1-(5-chlorothiophen-2-yl)-3-(2,3-dichlorophenyl)prop-2-en-1-one (CTDCP) [93]	16.21
2-(4-methylphenoxy)-N0-[(1E)-(4-nitrophenyl)methylene]acetohydrazide (4MNA) [94]	10.24
1-(4-aminophenyl)-3-(3,4,5-trimethoxyphenyl)prop-2-en-1-one (APTP) [95]	8.70
(2E)-3-[4-(methylsulfanyl)phenyl]-1-(4-nitrophenyl)prop-2-en-1-one (4N4MSP)[96]	2.37
(2E)-1-(4-bromophenyl)-3-[4-methylsulfanyl)phenyl]prop-2-en-1-one (4Br4MSP)[96]	2.30
(2E)-1-(3-bromophenyl)-3-[4 (methylsulfanyl) phenyl]prop-2-en-1-one (3Br4MSP)[96]	1.99

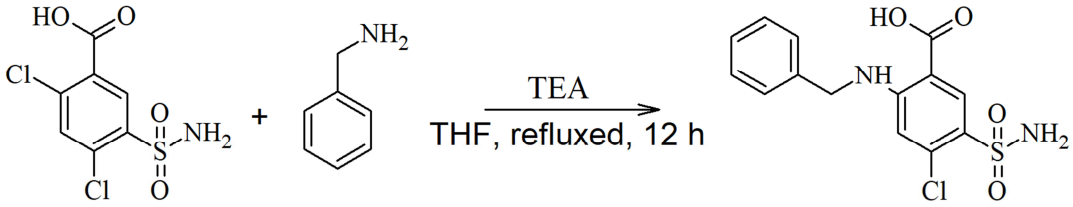

Scheme -1: Synthetic scheme for 2-(benzylamino)-4-chloro-5-sulfamoylbenzoic acid (BACSBA).

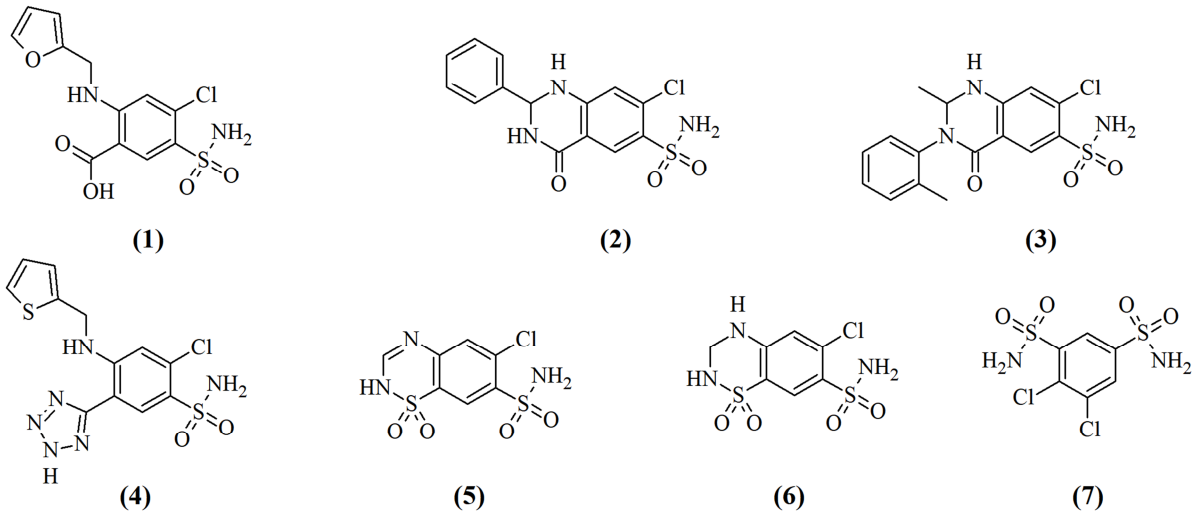

Figure 1. Some potent biologically active chlorosulfonamide drug moieties.

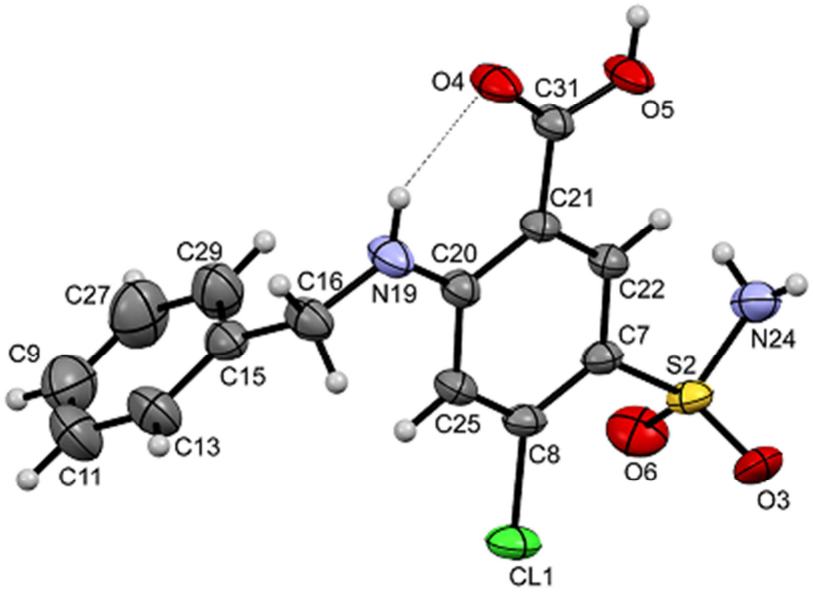

Figure 2. ORTEP view of 2-(benzylamino)-4-chloro-5-sulfamoylbenzoic acid (BACSBA) with thermal ellipsoids drawn at 50% probability.

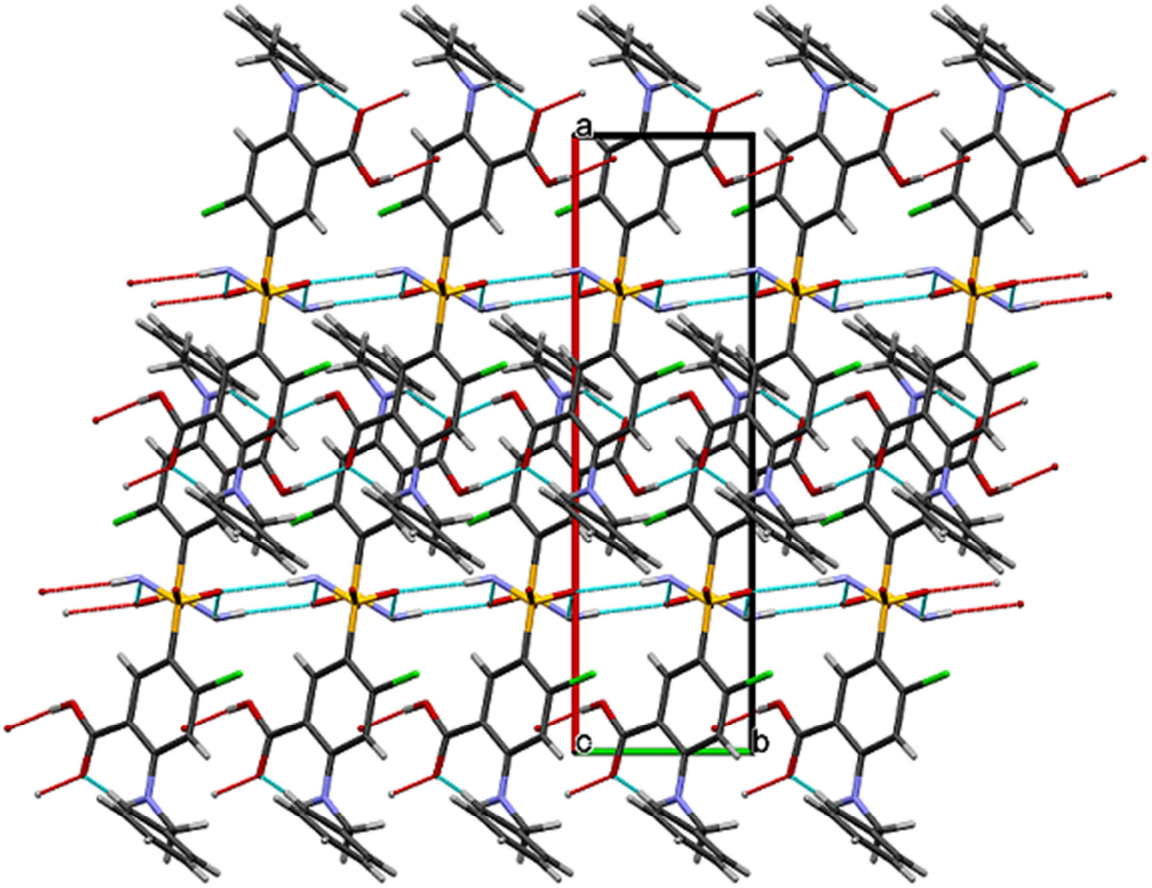

Figure 3. Packing of molecules in the crystal lattice of BACSBA.

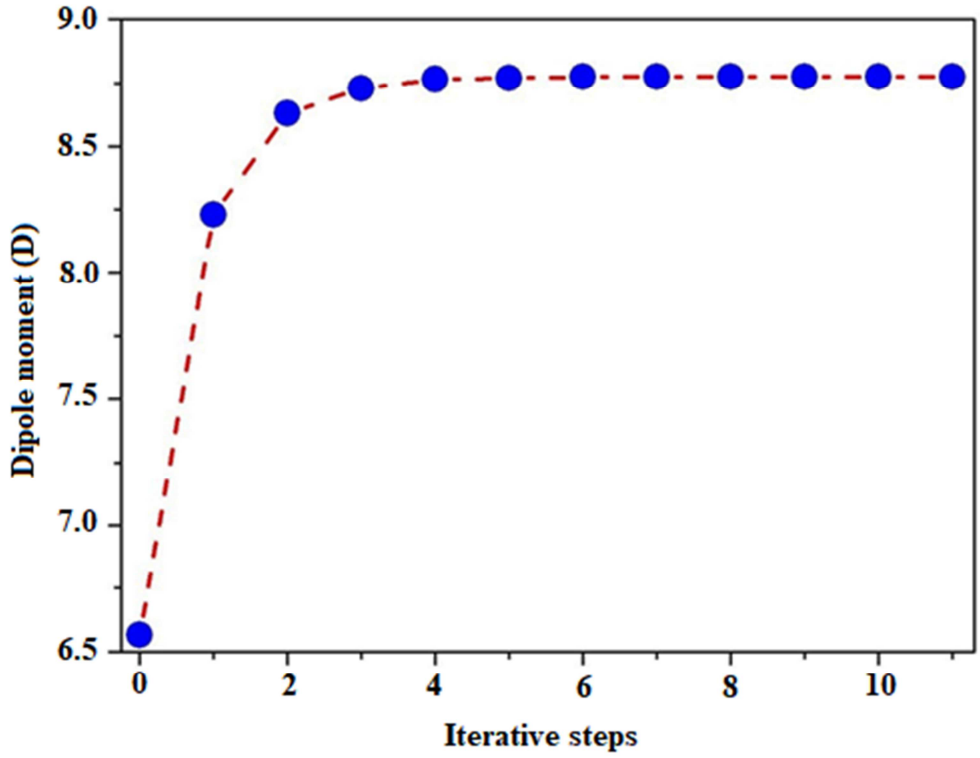

Figure 4. Dipole moment values as function of the iterative steps.

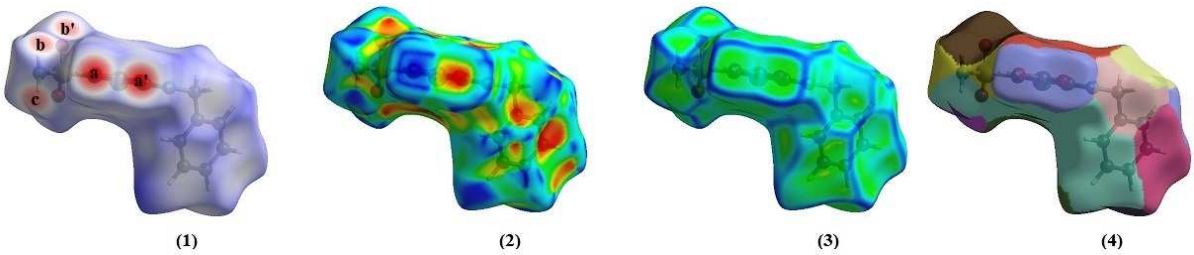

(a) Hirshfeld surfaces of BACSBA: d_{norm} (1), *shape index* (2), *curvedness* (3), *fragment patch* (4).

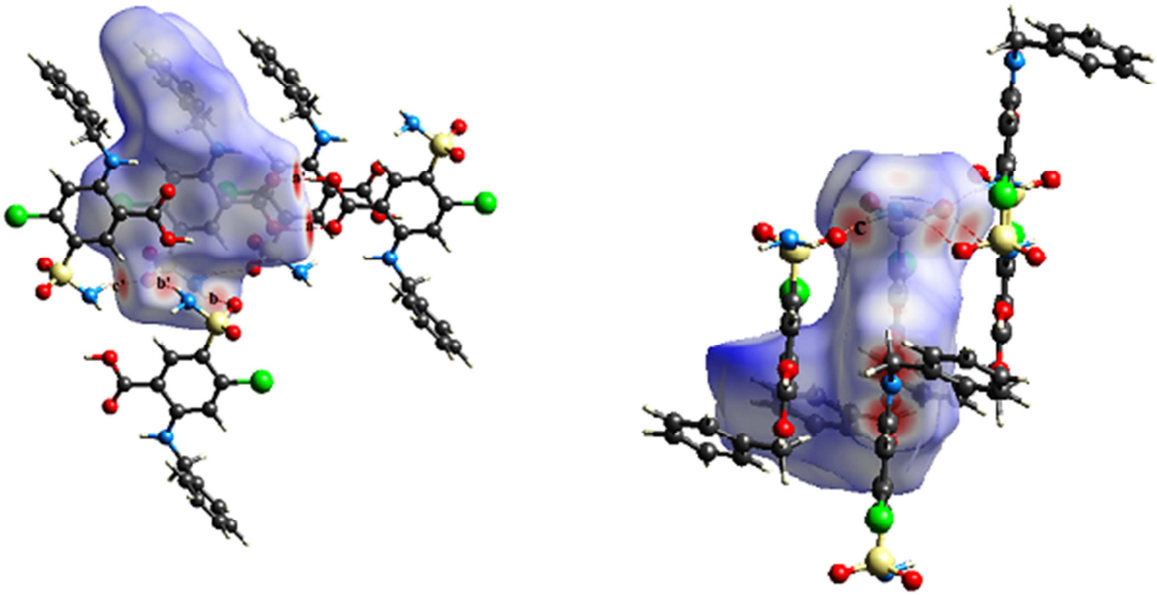

(b) View of O---H interactions.

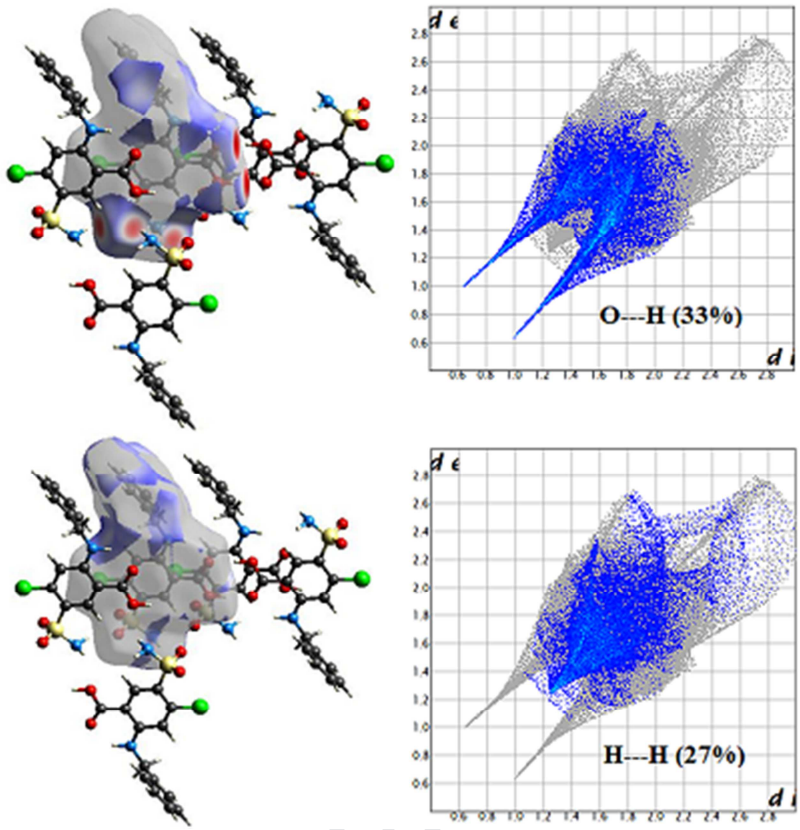

(c) Finger print plots of the BACSBA compound and major interactions visualized with percentage (i) O---H interactions (33%) and H---H interactions (27%).

Figure 5. Analysis of 3D-Hirshfeld surfaces and 2D-finger print plots of BACSBA molecule.

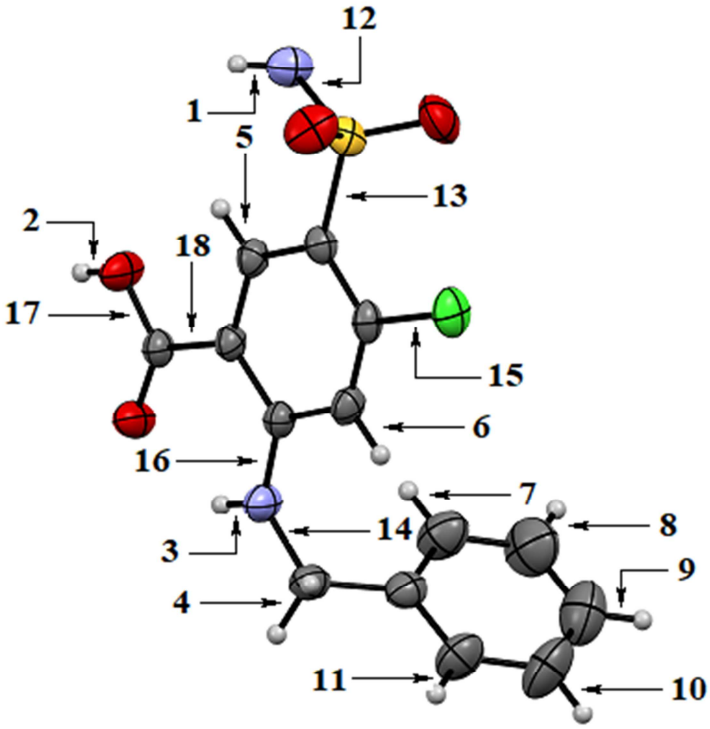

Bond Number	BDE[kcal/mol]
1.	105.07575
2.	91.57676
3.	97.12646
4.	86.73929
5.	108.86026
6.	111.54098
7.	110.62293
8.	110.5081
9.	111.02642
10.	110.5721
11.	110.20062
12.	54.08317
13.	61.777692
14.	70.643775
15.	81.530443
16.	98.135598
17.	100.41409
18.	105.12982

Figure 6. H-BDE (violet color) and BDE (green color) values for BACSBA molecule.

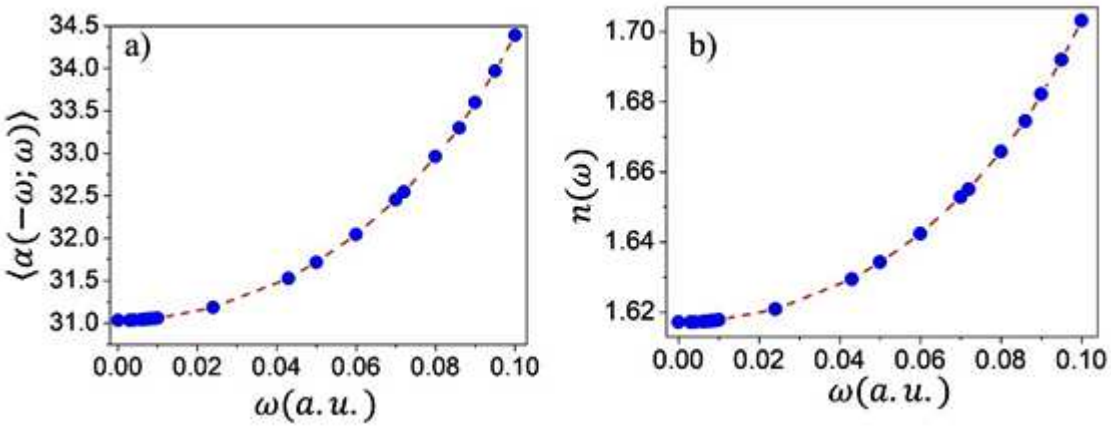

Figure 7. Linear polarizability and linear refractive index as function of the electric field frequencies.

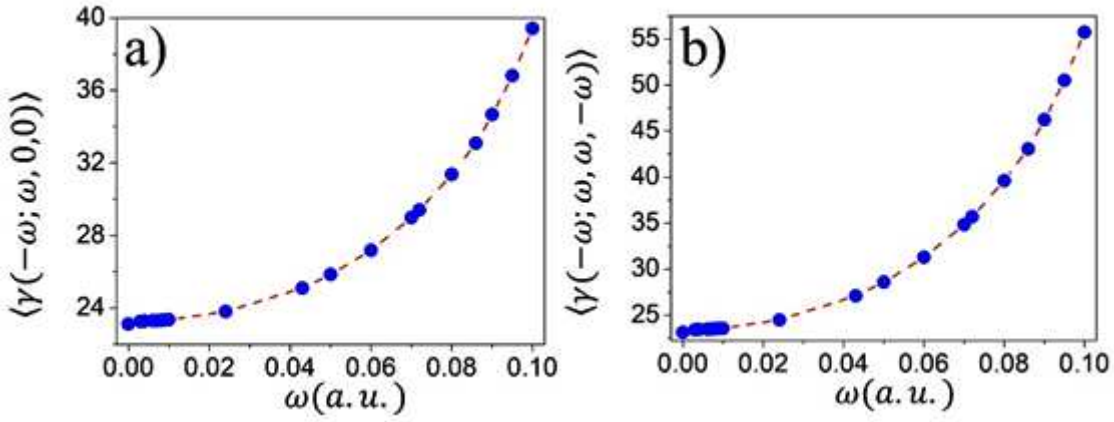

Figure 8. Second hyperpolarizabilities $\langle\gamma(-\omega;\omega,0,0)\rangle$ and $\langle\gamma(-\omega;\omega,\omega,-\omega)\rangle$ ($in\ units\ of\ 10^{-36}esu$) as function of the electric field frequencies.

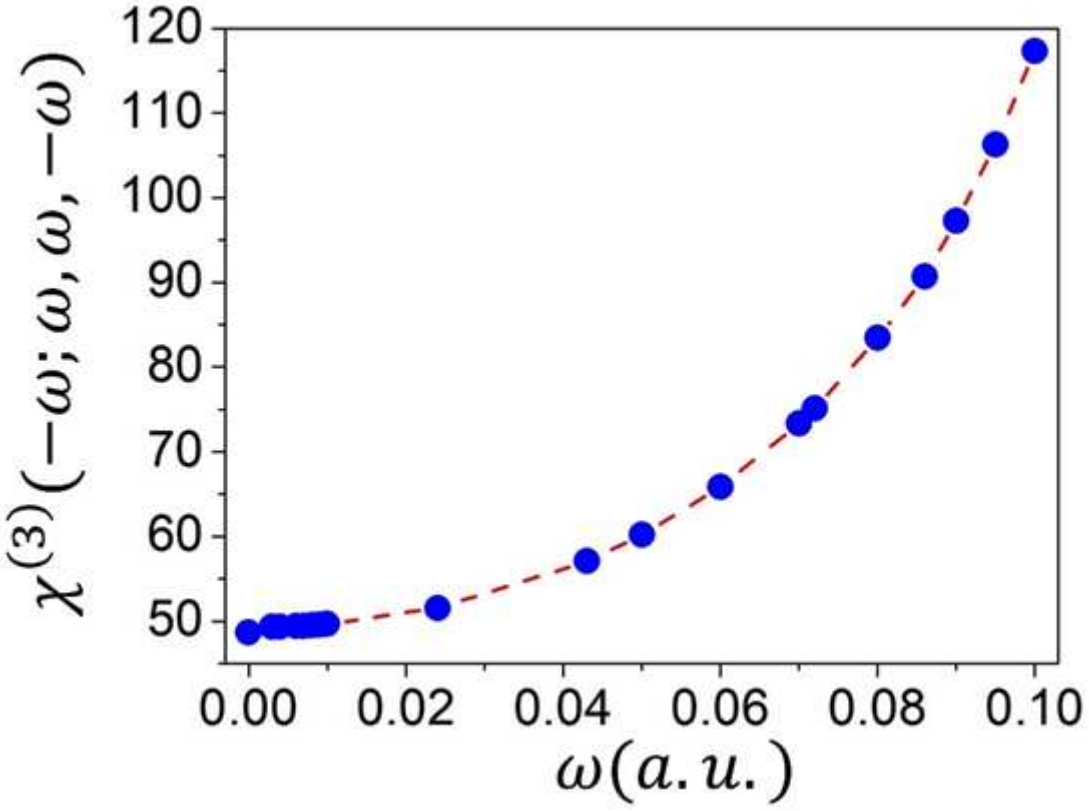

Figure 9. Third-order nonlinear susceptibility ($10^{-22}m^2/V^2$) as function of the frequency.

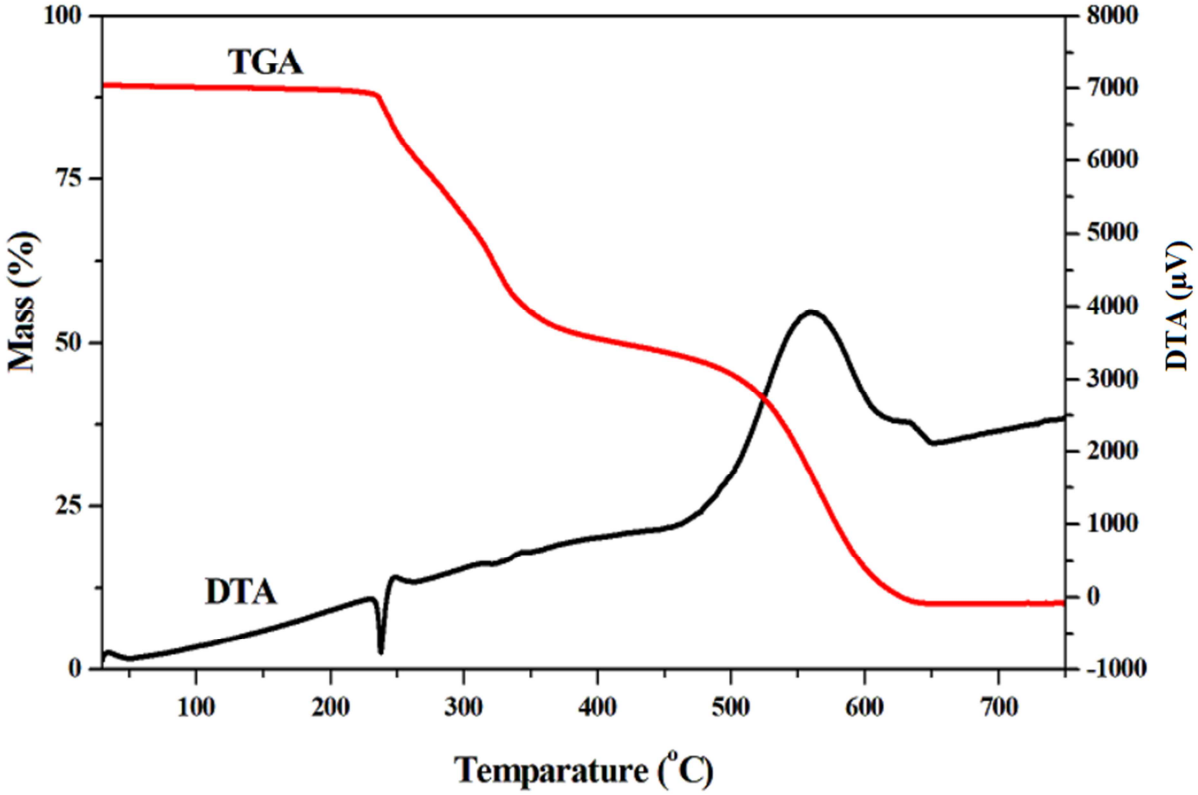

Figure 10. DTA/TGA graph of BACSBA compound.

Highlights

- The L-shaped molecular structure of the BACSBA was confirmed by single crystal X-ray diffraction technique and Quantum chemical methods.
- Most reactive sites are identified.
- Bond dissociation energies are calculated in order to predict possible degradation properties.
- BACSBA crystal is an attractive object for further studies on nonlinear optics.
- Antifungal and antioxidant studies are reported.

Title of the manuscript: An analysis of spectroscopic, computational and biological activity studies of L-shaped sulfamoylbenzoic acid derivatives: A third order nonlinear optical material

Declaration of interests

There was no potential conflict of interest declared by authors.